LLNL-JRNL-2011687

Lawrence Livermore National Laboratory

Temporal relationship Among Lunar Crustal rocks

T Kruijer, A Roberts, L Borg, M Liu, O Maina, J Wimpenny, J Boro

February 2026

Geochemica et Cosmochemica Acta

Disclaimer

This work performed under the auspices of the U.S. Department of Energy by Lawrence Livermore National Laboratory under Contract DE-AC52-07NA27344.

Geochimica et Cosmochimica Acta

Temporal Relationship Among Lunar Crustal Rocks

--Manuscript Draft--

Manuscript Number:	GCA-D-25-00650R1
Article Type:	Article
Keywords:	Moon, highlands crust, chronology, isotopes, zircons
Corresponding Author:	Lars Borg, Ph. D Lawrence Livermore National Laboratory Livermore, California UNITED STATES
Corresponding Author's Institution:	Lawrence Livermore National Laboratory
First Author:	Lars Borg, Ph. D
Order of Authors:	Lars Borg, Ph. D
	Thomas Kruijer
	Ming-Chang Liu
	Autumn Roberts
	Josh Wimpenny
	Ouyanatu Maina
	Joseph Boro
	Charles Shearer
	Kyle Samperton
Abstract:	Temporal relationships among the three most common suites of lunar crustal rocks have been investigated by obtaining high precision ages on a Felsic/Alkali-suite clast from breccia 15405 and Magnesian-suite norite 78236/8/55/56 and comparing them to previously dated ferroan anorthosite sample 60025. The weighted average age of 4337.19 ± 0.49 Ma of Clast B, defined by zircon U-Pb and Pb-Pb ages as well as mineral isochron Sm-Nd and Nd-Nd ages, is nearly identical to the weighted average age for Apollo 17 norite 78236/8/55/56 of 4334.1 ± 3.5 Ma, defined by Pb-Pb ages measured on baddeleyites in this investigation and less precise Pb-Pb and Sm-Nd ages previously reported. Both ages are ~25 Ma younger than the weighted average of Sm-Nd and Pb-Pb ages reported by Borg et al. (2011) on ferroan anorthosite 60025 of 4359.3 ± 2.3 Ma. The fact that ages on all three samples are defined by multiple U-Pb, Pb-Pb, Sm-Nd, and Nd-Nd chronometers suggests they record the igneous crystallization history of the samples and do not represent disturbances or mixing lines with no temporal significance. The extent to which these three ages represent broader scale magmatism is difficult to evaluate. Nevertheless, the age defined for 15405 Clast B, 78236/8/55/56, and 60025 are contemporaneous with the peak of ages observed in detrital zircons from the Apollo 12, 14, 15, and 17 landing sites (4340 ± 20 Ma), a Mg-suite Sm-Nd whole rock isochron defined by samples from Apollo 14, 15, 16, and 17 landing sites (4348 ± 25 Ma), and a ferroan anorthosite-suite Sm-Nd whole rock isochron defined by samples from Apollo 15 and 16 landing sites (4354 ± 29 Ma). This implies that primordial Ferroan Anorthosite-suite magmatism is temporally distinct from secondary magmatism associated with the Mg-suite and the Felsic/Alkali-suite, as predicted by the lunar magma ocean model of lunar differentiation. The short interval between primordial ferroan anorthosite magmatism and secondary magmatism suggests that the lunar crust formed over a limited period of time. Although heat from radiogenic decay of long-lived isotopes, large impacts, tidal heating associated with interactions between the Earth and Moon, and density driven overturn of the magma ocean have all been invoked to explain production of ancient secondary crustal magmatism, only tidal heating and cumulate overturn are consistent with the apparent short duration of secondary crustal magmatism and the great depth of crystallization implied for some Mg-suite samples.

	The initial ε143Nd values derived from the 15405 Clast B and 78238 Mg-suite norite isochrons, as well as a Mg-suite whole rock isochron are -0.23 ± 0.11, -0.27 ± 0.74, and -0.25 ± 0.09, respectively. They are identical within error indicating that Mg-suite and Felsic/Alkali-suite magmas were derived from materials that had the same time averaged Sm/Nd ratios since the formation of the solar system. This, combined with the contemporaneous nature of 15405 Clast B and 78236/8/55/56 Mg-suite norite, are consistent with evolution of both samples, and likely both magma suites, from a common source through closed system fractional crystallization or partial melting processes.
Response to Reviewers:	

Temporal Relationships Among Lunar Crustal Rocks

Lars E. Borg[a]*
Thomas S. Kruijer[a]
Ming-Chang Liu[a]
Autumn G. Roberts[a,b]
Josh Wimpenny[a]
Ouyanatu N. Z. Maina[a]
Joseph Boro[a]
Charles K. Shearer[c]
Kyle M. Samperton[a,d.]

a. *Cosmochemical & Isotopic Signatures Group, Lawrence Livermore National Laboratory, 7000 East Avenue L-231, Livermore, CA 94550, USA*
b. *Geological Sciences, University of Colorado, Boulder, CO 80309, USA*
c. *Department of Earth and Planetary Science, Institute of Meteoritics, University of New Mexico, Albuquerque, NM 87131, USA*
d. *Trace Nuclear Measurement Technology Group, Savannah River National Laboratory, Aiken SC, 29802 USA*

Corresponding author: borg5@llnl.gov

Abstract

Temporal relationships among the three most common suites of lunar crustal rocks have been investigated by obtaining new high precision ages on Felsic/Alkali-suite Quartz monzodiorite Clast B from breccia 15405 and Magnesian-suite norite 78235/6/8/55/56 and comparing them to previously dated ferroan anorthosite sample 60025. The weighted average age of 4337.19 ± 0.49 Ma of 15405 Clast B is defined by zircon U-Pb and Pb-Pb ages as well as mineral isochron Sm-Nd and Nd-Nd ages. It is identical to the weighted average age for Apollo 17 norite 78235/6/8/55/56 of 4334.1 ± 3.5 Ma which is defined by Pb-Pb ages measured on baddeleyites in this investigation and less precise Pb-Pb and Sm-Nd ages reported in the literature. Both ages are ~25 Ma younger than the weighted average of Sm-Nd and Pb-Pb ages reported in the literature on ferroan anorthosite 60025 of 4359.3 ± 2.3 Ma. The fact that ages of all three samples are defined by multiple U-Pb, Pb-Pb, Sm-Nd, and ^{142}Nd-^{143}Nd chronometers provide confidence that they record the igneous crystallization history of the samples and do not represent disturbances or mixing lines with no temporal significance.

The extent to which these three ages represent broader scale magmatism is difficult to evaluate. Nevertheless, the age defined for 15405 Clast B, 78235/6/8/55/56, and 60025 are contemporaneous with the peak of ages observed in detrital zircons from the Apollo 12, 14, 15, and 17 landing sites (4340 ± 20 Ma), a Mg-suite Sm-Nd whole rock isochron defined by samples from Apollo 14, 15, 16, and 17 landing sites (4348 ± 25 Ma), and a Ferroan Anorthosite-suite Sm-Nd whole rock isochron defined by samples from the Apollo 15 and 16 landing sites (4354 ± 29 Ma). This implies that Ferroan Anorthosite-suite magmatism is temporally distinct and earlier than magmatism associated with the Mg-suite and the Felsic/Alkali-suite, as predicted by the lunar magma ocean model of lunar differentiation. The short 35 ± 10 Ma interval between primary

ferroan anorthosite magmatism and secondary magmatism suggests that the lunar crust formed over a limited period of time. Although heat from decay of long-lived isotopes, large impacts, tidal heating associated with interactions between the Earth and Moon, and density driven overturn of the magma ocean have all been invoked to explain production of ancient secondary crustal magmatism, only tidal heating and cumulate overturn are consistent with the apparent short duration of secondary crustal magmatism and the great depth of crystallization implied for some Mg-suite samples.

The initial ε^{143}Nd values derived from the 15405 Clast B and 78238 Mg-suite norite isochrons, as well as a Mg-suite whole rock isochron are -0.23 ± 0.11, -0.27 ± 0.74, and -0.25 ± 0.09, respectively. They are identical within uncertainty indicating that Mg-suite and Felsic/Alkali-suite magmas were derived from materials that had the same time averaged Sm/Nd ratios since the formation of the solar system. This, combined with the contemporaneous nature of 15405 Clast B and 78235/6/8/55/56 Mg-suite norite, is consistent with evolution of both samples, and likely both magma suites, from a common source through closed system fractional crystallization or partial melting processes.

1. Introduction

The ancient lunar crust is thought to be comprised of three major lithologies (Figure 1) that include the Ferroan Anorthosite-suite (FAS), the Magnesian-suite (MGS), and the Alkali-suite (AKS; e.g., Shearer et al., 2006; 2015). The FAS represents flotation cumulates produced after ~80% crystallization of the Lunar Magma Ocean (LMO; e.g., Walker et al. 1975, Warren 1985, Snyder et al. 1992, Elkins-Tanton et al. 2011, Elardo et al. 2011, Lin et al. 2017, Rapp & Draper

2018). This conclusion is based on the observation that rocks of this suite are widespread on the lunar surface and are characterized by high Ca and Fe abundances, but low Mg abundances (e.g., Wood et al., 1970). In contrast, the other crustal suites (MGS and AKS) contain a component known as KREEP, because it is enriched in K, REE, and P, that is considered to be a very late-stage crystallization product of the LMO that post-dates production of FAS (Warren and Wasson, 1979). The inferred petrogenesis of these three suites of rocks implies that the FAS is a primordial crystallization product of the LMO and should therefore be older than either the MGS or the AKS that are KREEP-rich and thus expected to be produced in secondary crust forming events. However, previous age determinations of FAS and MGS crustal rocks, as well as detrital zircons inferred to be derived from the AKS, do not conform to the temporal relationship predicted from the chemical stratigraphy of the LMO model (Figure 2). Instead, it is apparent that the ages of the FAS and MGS overlap from about 4.30 to 4.55 Ga. Previously reported AKS ages, defined almost exclusively by detrital zircons, range from 3.90 to 4.45 Ga and thus mostly overlap the ages of the MGS and FAS. If these ages are taken at face value, significant modification or even abandonment of the LMO model is required to accommodate the apparent contemporaneous emplacement of the three crustal magmatic suites.

A detailed examination of Figure 2, however, demonstrates that not all the published sample ages are reliable or useful to delineate closely spaced magmatic events. Many of the ages determined on individual samples have extremely large uncertainties, with the oldest FAS and Mg-suite rocks yielding errors as large as 150 Ma (see summaries in Borg et al., 2015; Papike et al., 2018; Borg and Carlson, 2022). In addition, many samples that have been dated by multiple research groups using different chronometers frequently are not concordant (Figure 2). In retrospect, it is not possible to understand why these differences exist from the limited technical

information in the literature, but there are a variety of possibilities. The mechanisms most commonly invoked include isotopic disturbance by impact processes, different approaches to neutron capture corrections to the Sm-Nd system, variable closure temperatures of different chronometers, and the relatively poor precision of some chronometric measurements (Borg et al., 2015; Papike et al., 2018; Borg and Carlson, 2022).

Much of the ambiguity in the determination and interpretation of lunar crustal rock ages can be alleviated by obtaining concordant high precision ages on single igneous samples across multiple chronometric systems. This is based on the principle that isotopic disturbances of lunar samples are very unlikely to reset different isotopic systems without complete remelting of the samples. Remelting by impacts is relatively easily identified through petrologic examination and the presence of meteoritic contamination of siderophile elements. Obtaining multiple concordant ages using multiple isotopic systems thus provides confidence that measured ages reliably date igneous crystallization without relying on indices associated with the measured isotopic systematics, such as the quality of fit of the regression through the data, which has proven to be inconclusive (Nyquist et al., 1987; Gaffney et al., 2011).

Concordance between multiple chronometers does not address the low resolution of most isotopic systems, however. The Sm-Nd isotopic system has been the mainstay of lunar highland chronology because it is highly resistant to disturbance by impact processes (Nyquist et al., 1987; Gaffney et al., 2011). However, it lacks the analytical precision necessary to distinguish geologic events closely spaced in time. The U-Pb isotopic system is the only chronometer currently available to obtain absolute high precision ages on lunar highlands samples with uncertainties as low as 1-3 Ma. Nevertheless, the U-Pb system is not impervious to impact metamorphism and is often disturbed in highland samples (e.g., Tera and Wasserburg, 1972; Premo et al., 1999, Borg et

al., 2011). Therefore, in order to more tightly constrain the temporal relationships between the three lunar crustal rock suites we have applied a combination of ^{235,238}U-^{207,206}Pb, ^{207}Pb-^{206}Pb, and ^{146,147}Sm-^{142,143}Nd chronometers to an AKS clast (termed QMD Clast B) from lunar breccia 15405 as well as to MGS sample 78236/8. These ages are then compared to similar ages that were previously determined for FAS sample 60025 (Borg et al., 2011). The U-Pb system is used to provide high precision ages, whereas the Sm-Nd system is used to confirm that they are reliable and record igneous crystallization. This analysis demonstrates that lunar crustal magmatism appears to occur in discrete intervals separated by only a few tens of millions of years as predicted by the LMO model of planetary differentiation.

2. Sample descriptions

This investigation focusses on three representative samples from the FAS (ferroan anorthosite sample 60025), MGS (norite sample 78235/6/8/55/56), and AKS (quartz monzodiorite sample 15405 Clast B). Their petrologic characteristics are briefly described below.

2.1 Quartz Monzodiorite Clast B

Quartz Monzodiorite (QMD) Clast B was entrained in impact melt breccia 15405. It was chipped off the top of a boulder found on the Apennine Front at Station 6A of the Apollo 15 landing site. It contains several lithic fragments including KREEP-basalts and granites, as well as quartz-monzodiorites (Ryder; 1976; Ryder and Wood, 1976). Although this impact melt breccia sample originally contained three labeled QMD clasts (A, B, and C; Ryder, 1976; Ryder and Norman, 1979; Taylor et al., 1980; Takeda et al., 1981), much of this material has been exhausted. Our subsample, (,272), was removed from slab 91 after it was retrieved from remote storage in White

144 Sands NM. It contained the second part of Clast B that was exhausted from slab 95 originally
145 stored at the Johnson Space Center.

146 Clast B is very similar to other QMD samples described in the literature (e.g., Ryder and
147 Bower, 1976; Ryder, 1976; Takeda et al., 1981; Marvin et al., 1991; Ryder and Martinez, 1991;
148 Jolliff, 1991). Our portion of Clast B (Figure 3) is coarse-grained and contains plagioclase ($An_{77-87}Ab_{13-21}Or_{1}$), K-feldspar ($An_{2-4}Ab_{6-11}Or_{82-93}$) with intergrown quartz in a texture reminiscent of
149 granophyric intergrowths, orthopyroxene ($En_{31-33}Fs_{64-66}Wo_{2-3}$) and exsolved clinopyroxenes ($En_{29-31}Fs_{51-59}Wo_{10-17}$) as well as ($En_{26-27}Fs_{31-36}Wo_{38-43}$), with minor amounts of ilmenite, phosphate,
150 zircon, baddeleyite, zirconalite, Fe-Ni metal, and fayalitic olivine (Fo_{17-21}). Although we did not
151 determine the width of exsolution lamellae in Clast B, they appear to have widths that are roughly
152 similar to those measured in a 15403 QMD fragment of ~2 μm (McCallum and O'Brien, 1996).
153 Representative mineral compositions are presented in the supplement (Table S1). The
154 compositions of the minerals in Clast B are very similar to those reported for other Apollo 15 QMD
155 clasts (Ryder, 1976; Takeda et al., 1981; Marvin et al., 1991; Ryder and Martunez, 1991; Meyer et
156 al., 1996; Fagan et al., 2014). Takeda et al. (1981) found evidence for intragranular melting in
157 some pyroxene crystals in Clast A that they interpreted as a response to impact shock. Our portion
158 of Clast B also demonstrated evidence for intragranular melting in the pyroxene and is expressed
159 as veins comprised of a mixture of pyroxene, feldspar, oxides, and Fe-rich olivine. Nevertheless,
160 the coarse-grained texture and low siderophile element abundances of the QMD lithology in 15405
161 indicates that it represents a pristine (i.e. minimally altered by impact processes) igneous lithology
162 (Gros et al., 1976; Ryder, 1976; Marvin et al., 1991; Warren, 1993).

163 Major and trace element abundances were determined on a ~6 mg aliquot derived from the
164 <325 mesh sieve split that is labeled Wr-1 in Table S2. The major element composition of the Wr-

1 split is somewhat more felsic than the compositions determined on other QMD clasts by Taylor et al. (1980) and Fagan et al. (2014) having SiO_2 of 63.7 wt.% compared to 44.8-60.1 wt.%. Although Clast B also has higher Al_2O_3 and lower FeO and MgO, the MgO/(MgO+FeO) on all of the 15405 QMD clasts is nearly identical, ranging from 0.20 to 0.22 (Taylor et al., 1980; Fagan et al., 2014; this study) consistent with a common heritage (Ryder and Bower, 1976). An estimate of the mineral mode of Clast B calculated using the measured whole rock and mineral compositions indicates it is comprised of approximately 38% plagioclase, 28% quartz, 13% K-feldspar, 13% orthopyroxene, 6% clinopyroxene, and ~1% each of ilmenite and phosphate. According to the International Union of Geological Sciences (IUGS) QAPF (Quartz-Alkali Feldspar-Plagioclase-Feldspathoids) classification developed by Streckeisen (1976), the calculated mineral mode of Clast B technically makes it a granodiorite, not a monzodiorite. However, given the small size of individual samples, the extremely heterogeneous mineral modes, and to maintain consistency with previous work, we have adopted the conventional QMD nomenclature.

The trace element composition of Clast B is similar to other QMD clasts. The proportions of REE in the various samples of QMD lithology, as well as that of KREEP basalts, such as 15386, are identical (Figure 4), reflecting the high proportion of urKREEP in these samples. However, although Clast B is very strongly enriched in REE elements, absolute abundances are lower than those observed in Clast A by Taylor et al. (1980), Nyquist et al. (1976a, 1976b), and Ryder (1976). This probably reflects the highly variable modal abundance of phosphate in the QMD lithology, which ranges up to 18% (Marvin et al., 1991).

2.2 Norites 78235/6/8 and 78255/6

Norites 78235, 78236, 78238, 78255 and 78256 (78235/6/8/55/56) are related samples from the same boulder found at Apollo 17 Station 8 site (Meyer, 1994). Samples 78236 and 78238 are from adjacent areas on the top of a boulder whereas sample 78255 was chipped from the bottom of the boulder. This sample set has been extensively studied so only a brief summary of its petrographic characteristics is presented here. Sample 78235/6/8, as well as sample 78255/6, are course-grained cumulate norites containing 30-60% orthopyroxene, 40-60% plagioclase, and trace amounts of clinopyroxene, silica, apatite, merrillite, glass, baddeleyite, and zircon (Jackson et al., 1975; McCallum and Mathez, 1975, Dymek et al., 1975; Steele 1975; Hinthorne et al., 1977). Mineral sizes range from about 2 mm to 1 cm (Jackson et al., 1975). It is heavily shocked (Sclar and Bauer, 1975, 1976) as indicated by the presence of impact melt veins, brecciated texture, and conversion of some of the plagioclase to the diaplectic glass maskelynite. Mineral compositions are typical of Mg-suite norites (see McCallum and Mathez, 1975; Dymek et al., 1975. Despite the presence of shock features, 78235/6/8/55/56 has low siderophile element abundances and, like the QMD Clast B, is considered to be pristine (Warren, 1993).

2.3 Ferroan anorthosite suite sample 60025

Although the crystallization age of FAS sample 60025 was published previously (Borg et al., 2011), a brief description of this lithology is presented here because it is the only precisely dated FAS sample and consequently serves as a key point of comparison for other lunar crustal rock ages measured in this investigation. Sample 60025 is a moderately shocked cataclastic ferroan anorthosite composed predominantly of anorthositic plagioclase (An_{96-98}) and orthopyroxene ($En_{49-72}Fs_{28-48}Wo_{2-6}$) and clinopyroxene ($En_{35-46}Fs_{9-21}Wo_{42-46}$). It is relatively coarse grained with some plagioclase and pyroxene up to 4 mm in size. The relatively wide range of pyroxene compositions has been interpreted as both a result of subsolidus exsolution (Smith

and Steele, 1974) and continuous closed system crystallization of an evolving parental liquid (Ryder, 1982; James et al., 1991). In either case, the mineral phases in 60025 are expected to have the same initial isotopic compositions and therefore to be in isotopic equilibrium. The pyroxene compositions have also been interpreted as a result of mixing two similar, but unrelated, rocks (Floss et al., 1998). However, the concordance of the Sm-Nd age determined on plagioclase and pyroxene and the Pb-Pb age determined solely on pyroxene (Borg et al., 2011) demonstrates that this is not possible unless the two lithologies have the same age and initial $^{143}Nd/^{144}Nd$ ratios.

3. Methods

We performed petrographic and geochemical characterizations of AKS sample 15405 that augment the existing data, as well as $^{235,238}U$-$^{207,206}Pb$, ^{207}Pb-^{206}Pb, and $^{146,147}Sm$-$^{142,143}Nd$ chronologic measurements. In addition, we have completed ^{207}Pb-^{206}Pb SIMS age determinations on baddeleyites from MGS sample 78235/6/8-78255 to supplement less precise U-Pb, Pb-Pb, Rb-Sr, and Sm-Nd ages in the literature. The techniques applied to each sample are briefly outlined below and discussed in detail in the supplementary materials.

3.1 Sample preparation for 15405 QMD Clast B

The aliquot 15405 weighed 496 mg and was composed of both dark matrix impact melt material and a fragment of Clast B. The clast was removed from impact melt matrix material using a steel probe and a binocular microscope. Matrix-free Clast B material consisted of about five QMD fragments each with well-defined borders. Three of these fragments were gently crushed in a sapphire mortar and pestle and then sorted by grain size using nylon sieves at 100-200 mesh (150-75 microns), 200-325 mesh (74-44 microns), and <325 mesh. One of the remaining two

fragments (Figure 3) was mounted in a potted butt for electron microprobe and secondary ion mass spectrometry analysis. The final fragment weighing ~17 mg was held in reserve.

3.2 Chronologic Measurements QMD Clast B and MGS Norite

Mineral separates for Rb-Sr and Sm-Nd isotope measurements of QMD Clast B were prepared from the 100-200 mesh size fraction using a Frantz magnetic barrier separator and hand-picking. The fractions were digested in a combination of HCl and HF. Major and trace elements were determined on 5% aliquots of these digestions and the remainder was processed through Rb-Sr and Sm-Nd ion chromatography procedures described in Borg et al. (2020). The U-Pb and Pb-Pb age determinations of Clast B zircons were determined using chemical abrasion-isotope dilution thermal ionization mass spectrometry (Mundil et al., 2004; Mattinson, 2005). Zircons were extracted from the 200-325 mesh sized fraction after identification using the secondary electron microscope. They were thermally annealed at 900 °C, chemically abraded, and sequentially digested to yield two leachates and one residue fraction per zircon. All fractions were spiked using the mixed BSU1b ^{205}Pb-^{233}U-^{235}U tracer. This tracer was previously calibrated against similar gravimetric reference materials as used for the EARTHTIME tracers (Condon et al., 2015; McClean et al., 2015). Uranium and Pb were isolated using ion chromatography following the procedures of Krogh (1973) and then analyzed by ID-TIMS at LLNL. This is the first time our laboratory has reported U-Pb ID-TIMS data from zircons so this procedure is described in detail in the supplementary materials.

Baddeleyites were identified in MGS norite thin sections 78238 ,13 and 78255 ,9 at the University of New Mexico. U-Pb dating of baddeleyite grains found in 78238 was conducted on the UCLA ims-1290 ion microprobe by adopting the method developed previously (Barboni et al.,

2017) with some modifications. More detailed description of the SIMS techniques is presented in the supplementary material.

4. Results

4.1 Age determinations on 15405 QMD Clast B and 782356/8/55/56 MGS Norite

4.1.1 QMD Clast B Pb-Pb zircon ages

A crystallization age of Clast B is obtained from both the ^{207}Pb-^{206}Pb (Figure 5) and U-Pb concordia intercept (Figure 6) measured on five zircons separated from the 200-325 mesh fraction. The zircon U-Pb data are presented in Table 1. The Pb-Pb ages are defined by zircon residue (R) fractions and range from 4335.1 ± 3.0 to 4338.4 ± 1.5 Ma with a weighted mean value of 4337.16 ± 0.76 Ma (95% CI, MSWD = 1.5, N = 5). The reported uncertainty for this age accounts for both analytical and tracer calibration uncertainties, but does not include uncertainty from the ^{235}U and ^{238}U decay constants. When decay constant uncertainty is included, the total uncertainty increases to ±8.9 Ma (2σ). The range of Pb-Pb ages determined on the L2 fractions (4260.7 ± 1.5 to 4320.8 ± 3.6 Ma) is more variable, reflecting higher relative blank contributions (Table 1). For example, the R fractions exhibit higher radiogenic to common Pb ratios (Pb^*/Pb_c, 9.5 to 197) compared to the L2 fractions (3.6 to 78). The Pb_c in the L2 fractions likely originates from multiple components, including laboratory blank contributions, surface contamination on the grains, and Pb from residual silicate mineral phases adhering to the grains. For this reason, determining the exact isotopic composition of the Pb_c in the L2 fractions is very challenging. This complexity, combined with the relatively low Pb^*/Pb_c ratios of some of the L2 fractions, leads to greater uncertainty of ages so that ages derived from the L2 fractions should be interpreted with caution.

It was assumed for the calculations that all Pb_c in the R fractions originated from laboratory blank with present-day terrestrial Pb_c isotopic composition as estimated from total procedure blanks at LLNL ($^{206}Pb/^{204}Pb$ = 18.058±0.285, $^{207}Pb/^{204}Pb$ = 15.337±0.277, $^{208}Pb/^{204}Pb$ = 37.293±0.519, 1s.d., N=15; see supplementary materials). However, it is also possible that some portion of the non-radiogenic Pb component was not modern Pb_c but rather ancient initial Pb inherited from the Moon. For instance, ZR-5 (R), the fraction with the lowest Pb^*/Pb_c of ~9.5, has a Pb_c abundance of 3.9 pg that is considerably elevated compared to the average laboratory blank value of 0.93 ± 0.50 pg derived from analyses of Temora-2 zircons (Table S3). Deciphering the cause of the anomalously elevated Pb_c of ZR-5 is not straightforward but might reflect unaccounted silicate mineral phases adhering to this zircon. Regardless of the exact cause, the Pb-Pb age for this sample is identical within uncertainty to that of the other R fractions. The effect of the assumed isotopic composition of Pb_c is evaluated for each of the analyzed zircon R fractions. For these calculations two potential initial Pb compositions were considered: (1) common Pb incorporated at 4.34 Ga following the Pb evolution model of Stacey and Kramers (1975) and (2) an initial lunar Pb composition incorporated at 4.34 Ga assuming prior Pb growth occurred in a reservoir with elevated U/Pb (μ-value of 100). The $^{207}Pb/^{206}Pb$ ages of the R fractions, calculated using different assumptions for initial Pb contributions and compositions, are summarized in Table S4. Despite assuming very different Pb_c isotopic compositions, the resulting $^{207}Pb/^{206}Pb$ ages of four zircons (ZR-1, ZR-4, ZR-8, ZR-11) were identical within analytical uncertainty across all scenarios. The only significant variation in age calculations was observed for ZR-5, which has by far the lowest Pb^*/Pb_c ratio. For this sample, the calculated $^{207}Pb/^{206}Pb$ age varied by up to 45 Ma depending on the assumed common Pb composition. Nevertheless, an important result of these calculations is that all five R fractions yield

indistinguishable $^{207}Pb/^{206}Pb$ ages when the common Pb is assumed to be only modern terrestrial Pb. This consistency strongly suggests that the zircon R fractions lack any significant initial Pb and that the measured common Pb is entirely modern terrestrial Pb. For this reason, the reported ^{207}Pb-^{206}Pb ages of all lunar zircons in this study were calculated assuming a modern terrestrial common Pb composition.

4.1.2 U-Pb concordia ages for 15405 QMD Clast B zircons

A concordia diagram of the U-Pb results for zircons from 15405 QMD Clast B is given in Figure 6. The U-Pb data for the 15405 zircons exhibit significant variations in their radiogenic $^{207}Pb/^{235}U$ and $^{206}Pb/^{238}U$. While some residue (R) fractions plot near the concordia, all L2 fractions and some R fractions plot away from the concordia towards lower $^{207}Pb/^{235}U$ and $^{206}Pb/^{238}U$. This suggests that the U-Pb systematics of several zircons were disturbed as a result Pb loss in association with post-crystallization processes occurring either on the lunar surface or in the laboratory. Consistent with this, the ^{235}U-^{207}Pb and ^{238}U-^{206}Pb ages are strongly discordant for all but one of the L2 fractions, rendering these ages unreliable and of questionable geological significance. In contrast, a subset of five R fractions (ZR-1, ZR-4, ZR-5, ZR-8, ZR-11) plot considerably closer to the concordia and appear to define a discordia array, with three fractions (ZR-1, ZR-8, and ZR-11) plotting very close to the concordia (see inset in Figure 6). The upper intercept of a line regressed through these five points yields an age of 4337.49 ± 0.95 Ma (95% CI, N = 5, MSWD = 1.4), which is identical to the average $^{207}Pb/^{206}Pb$ age of 4337.15 ± 0.76 Ma derived earlier (Figure 5).

Evidence for secondary alteration is evident in the petrology, Rb-Sr, and even Sm-Nd isotopic systematics of Clast B (see below). The U-Pb concordia plots offer some temporal constraints on these events. Specifically, the five R fractions used in the discordia regression

(Figure 6) yield an imprecise lower intercept age of 116 ± 170 Ma (95% CI, MSWD = 1.4, N = 5). A more precise, but consistent, lower intercept age of 297 ± 62 Ma (95% CI, MSWD = 2.3, N = 6) is obtained when one of the L2 fractions (ZR-1 L2) is also included in the calculation. This implies that Pb was lost from Clast B zircon very recently. This may have been the event that excavated the QMD clast from depth or may have occurred as a result of processing in the laboratory.

Closer inspection of Figure 6 reveals even more complexity in the U-Pb systematics of the L2 fractions. This is expected given the fact that the L2 leaching step was implemented to preferentially dissolve zircons domains with more disturbed U-Pb systematics. While some L2 fractions (e.g., ZR-1, ZR-4) approximately align along the discordia calculated above for the R fractions, other L2 fractions (e.g., ZR-2, ZR-5, ZR-7, ZR 10) display greater scatter and even appear to define a second array on Figure 6. The isotopic systematics of the ZR-7 (L2) fraction offer some insights into the timing of secondary alteration events. It is the only L2 fraction that plots near (slightly above) the concordia, yielding nearly concordant $^{207}Pb/^{235}U$ and $^{206}Pb/^{238}U$ ages of 4306.8 ± 2.8 Ma and 4314.6 ± 6.7 Ma, respectively. However, despite yielding nearly concordant U-Pb ages, the ZR-7 (L2) ages are approximately 30 million years younger than the ~4337 Ma age obtained for the R fractions. Furthermore, while ZR-7 (L2) contained a measurable amount of radiogenic Pb (23 pg Pb*), the corresponding ZR-7 (R) fraction contained no Pb* and could not be analyzed. This suggests that the ZR-7 (L2) fraction may not represent a zircon but instead a more soluble Zr-bearing phase, that formed following a secondary disturbance of the rock. In this case the younger ~4.30 Ga age of ZR-7 (L2) might record the timing of a secondary alteration event occurring several tens of millions years after crystallization of Clast B. These interpretations are admittedly speculative. However, if they are

346 correct, it implies that QMD Clast B experienced multiple heating episodes which are important
347 to consider when examining the Rb-Sr and Sm-Nd isotopic systematics of Clast B.

348 *4.1.3 QMD Clast B Sm-Nd mineral isochrons*

349 The Sm-Nd isotopic systematics of lunar rocks are commonly modified by interactions of
350 galactic cosmic-rays with the lunar surface, producing thermal neutrons that are subsequently
351 captured by Sm and Nd isotopes (e.g., Nyquist et al., 1995). Thermal neutron production, and its
352 impact on the Sm-Nd isotopic systematics of individual samples, was monitored by measuring
353 the isotopic composition of Sm in the 15405 matrix that hosted Clast B. This approach takes
354 advantage of the large thermal neutron capture cross section of ^{149}Sm that drives the reaction
355 $^{149}Sm + n \rightarrow {}^{150}Sm + \gamma$. The measured Sm isotopic composition of 15405 matrix fraction was
356 determined to be $\varepsilon^{149}Sm = -0.77 \pm 0.12$ and $\varepsilon^{150}Sm = 1.95 \pm 0.18$ (where the ε-notation denotes
357 the 0.01% deviation of Sm isotope ratios from terrestrial standard values). These low values,
358 indicative of negligible neutron fluence, are consistent with the young exposure ages of 15405
359 determined using ^{21}Ne and ^{81}Kr by Drozd et al. (1976) that range from 6 Ma (no uncertainty
360 reported) to 11 ± 1.1 Ma, respectively. Minimum shifts in $\varepsilon^{149}Sm$ and $\varepsilon^{150}Sm$ are also consistent
361 with evidence for recent disturbance to the U-Pb system that implies that the sample may have
362 been brought to the surface in the last few millions of years. Importantly, the measured Sm
363 isotopic composition of 15405 matrix material indicates that any neutron capture corrections
364 made to the Sm-Nd isotopic systematics of the mineral fractions from Clast B are significantly
365 below the measurement uncertainties. For example, the correction for neutron capture on the
366 $^{147}Sm/^{144}Nd$ ratio results in an average -0.027% change of the ratio that is about four times
367 smaller than the analytical uncertainty of 0.1% associated with the measurement. Thus, Sm-Nd

isotopic systematics of sample 15405 are essentially unaffected by the capture of thermal neutrons.

Three ages have been calculated from the Sm-Nd data obtained on the mineral fractions from 15405 QMD Clast B using the data in Table 2. The ^{147}Sm-^{143}Nd isochron (Figure 7A) yields an age of 4329 ± 30 Ma and an initial εNd value of -0.23 ± 0.11 (MSWD = 0.86). This age is defined by the felsic, whole rock, leachate, and Mg-Px 2 fractions. The Fe-Px, Int-Px, and Mg-Px 1 fractions lie slightly below the regression indicating that the Sm-Nd isotopic system is disturbed (see inset in Fig. 7A). Mineral modes calculated from the major element compositions of these three mineral fractions demonstrate that they contain the highest proportion of pyroxene (40-70%), suggesting the Sm-Nd systematics of this phase has been disturbed. This is consistent with the petrologic evidence for intragranular melting in some pyroxene crystals in Clast B (Takeda et al., 1981). Despite the disturbance to the pyroxene-rich fraction, the 4329 ± 30 Ma age is interpreted to be the age of crystallization of Clast B because it is concordant with 4 other ages defined by the Sm-Nd and U-Pb systems (see below).

The second Sm-Nd isochron is defined by the ^{146}Sm-^{142}Nd decay chain (Figure 7B) yielding an age of 4334 ± 10 Ma (MSWD = 1.4). This age is calculated using the newly determined ^{146}Sm half-life of 92 Ma (Chiera et al., 2024). If the traditional half-life for ^{146}Sm of 103 Ma (Meissner et al., 1987) is used, the age derived from the ^{146}Sm-^{142}Nd isochron is 4301 $^{+11}/_{-12}$ Ma. Unlike the ^{147}Sm-^{143}Nd isochron, this isochron is defined by all of the mineral fractions, including the pyroxene-rich fractions. The reason the pyroxene-rich fractions lie on the isochron with the other fractions is that there is smaller variation in the ^{142}Nd/^{144}Nd ratio relative to the measured analytical uncertainty compared to the ^{143}Nd/^{144}Nd ratio, thus obscuring evidence for isotopic disturbance in this system. Furthermore, the fact that ^{146}Sm is almost

391 extinct when Clast B crystallized at ~4.33 Ga greatly minimizes the potential amount of
392 radiogenic ingrowth of ^{142}Nd occurring after a more recent disturbance. Thus, slight shifts of the
393 Sm/Nd ratios of phases resulting from late impact processes will have little or no effect on the
394 short-lived ^{146}Sm-^{142}Nd system, but a significantly larger effect on the long-lived ^{147}Sm-^{143}Nd
395 system.

396 The third age defined by the Sm-Nd system is based on ^{143}Nd-^{142}Nd (Borg et al., 2016).
397 This system yields an age of 4332 $^{+44}/_{-66}$ Ma (Figure 7C). Although not particularly precise, this
398 chronometer is not sensitive to recent disturbance of the Sm/Nd of the samples. Thus, like the
399 Pb-Pb system, it offers a means to assess the age of a sample like QMD Clast B that has been
400 subjected to impact metamorphism leading to remobilization of parent and daughter elements.
401 The Nd-Nd age is concordant with the other Sm-Nd ages and is consistent with crystallization of
402 Clast B around 4.33 Ga. The limited apparent disturbance of the ^{146}Sm-^{142}Nd system suggests
403 that crystallization was followed by a disturbance when this decay system was effectively
404 extinct, or nearly extinct, sometime after ~4.3 Ga. This is consistent with the age defined by the
405 ZR-7 (L2) fraction of ~4.30 Ga (see above), as well with the age of the Imbrium impact event
406 argued to have occurred around 3.94 Ga (Norman et al., 2006; Snape et al., 2016; Nemchin et al.,
407 2021).

408 In summary, the preferred crystallization age of Clast B from 15405 is the weighted
409 average of the U-Pb upper intercept age, the Pb-Pb age, and the three Sm-Nd ages of 4337.19 ±
410 0.49 Ma (MSWD = 0.19; N = 5).

411 *4.1.4 QMD Clast B Rb-Sr mineral isochrons*

412 The Rb-Sr isotopic data from QMD Clast B are presented in Table 3. The ^{87}Rb-^{86}Sr isotopic
413 system defines a semi-linear trend on a Rb-Sr isochron plot with a slope roughly corresponding to
414 an age of 4.34 Ga (Figure 8). However, Rb appears to have been extensively mobilized by impact
415 metamorphism so that the Rb-Sr chronometer does not yield any meaningful age information.
416 Plotting the Rb-Sr data from Clast A measured by Nyquist et al. (1976a, 1976b) along with data
417 from Clast B demonstrates a similar extent and style of Rb mobilization. Like the Sm-Nd system,
418 the disturbance of the Rb-Sr system most likely is a result of intragranular melting present in the
419 sample. The melting is most obvious in the pyroxenes, and the pyroxene-rich fractions lie farthest
420 from the 4337 Ma reference isochron in Figure 8.

421 Inspection of the inner granular areas in Clast B indicate they are comprised of a mixture
422 of pyroxene, feldspars, oxides, and Fe-rich olivine. This material must either be derived from a
423 melt originating outside the QMD lithology that had different Rb-Sr isotopic systematics than
424 Clast B or from a melt of QMD material that experienced Rb/Sr fractionation. The observation
425 that the pyroxene-poor mineral fractions lie on the opposite side of the 4337 Ma reference line to
426 the pyroxene-rich fractions suggests that the latter hypothesis is more likely.

427 **4.2 MGS Norite ages**

428 Six baddeleyite grains in a thin section of 78238 (,13) and two grains in a thin section from
429 78255 (,9) were dated in-situ. Two grains were large enough to accommodate three analysis spots.
430 In total, 12 zircon spot analyses of 78238 and 78255 were carried out. The $^{207}Pb/^{206}Pb$ and
431 $^{206}Pb/^{238}U$ ages are summarized in Table 4. The measured Pb signals are highly radiogenic
432 (≥98.7%), indicating that the surface cleaning method with pre-sputtering was effective. All the
433 Pb-Pb ages measured on eight grains in two thin sections agree within errors, yielding a well-
434 defined weighted mean and 2σ uncertainty of 4333.8 ± 3.7 Ma (N = 12, MSWD = 0.73). The ^{238}U-

435 ^{206}Pb and ^{235}U-^{207}Pb ages are also broadly consistent with the $^{207}Pb/^{206}Pb$ ages within uncertainty,
436 which yield weighted averages and errors of 4334 ± 65 Ma (N = 17/18, MSWD = 1.4) and 4344 ±
437 22 Ma (N=16/18, MSWD = 1), respectively. Given the higher precision, only the average ^{207}Pb-
438 ^{206}Pb age is used for the subsequent discussions.

439

440 **5. Discussion**

441 **5.1 Comparison to previously determined ages**

442 Uranium-Pb zircon SIMS ages have been previously determined from two thin sections of
443 15405 QMD clasts yielding values of 4294 ± 26 Ma (Meyer et al., 1996) and 4330 ± 6 Ma (Grange
444 et al., 2013). No mineral isochron data have been obtained on the QMD lithology. A lithology
445 similar to the QMD lithology was identified in meteorite NWA 2995 and dated by Pb-Pb and U-
446 Pb SIMS measurements in zircons and phosphates (Joy et al., 2025). They reported phosphate U-
447 Pb ages of 4317 ± 12 and 4321 ± 13 Ma and U-Pb zircon upper intercept age of 4330.6 ± 3.5 Ma.
448 Although Joy et al. (2025) interpret the evolved lithology in NWA 2995 to be South Pole–Aitken
449 basin impact melt, the lithology seems similar to, and the ages are concordant with, the 15405
450 QMD Clast B.

451 Unlike 15405 QMD Clast B, numerous crystallization ages have been determined on
452 MGS norite 78235/6/8-78255/6. Long-lived ^{147}Sm-^{143}Nd ages of 4340 ± 40 Ma (Carlson and
453 Lugmair, 1981), 4334 ± 37 Ma (Edmunson et al., 2009) and 4436 ± 51 Ma (Nyquist et al., 1981),
454 as well as Rb-Sr ages of 4355 ± 20 Ma (adjusted for $^{87}\lambda = 0.01397$) and 4381 ± 53 Ma
455 (Edmunson et al., 2009) have been determined. Mineral isochron and secondary ionization mass
456 spectrometry U-Pb and Pb-Pb ages of 4250 ± 90 Ma (Hinthorne et al., 1977), 4333 ± 59 Ma

(Edmunson et al., 2009), 4332 ± 18 Ga (Zhang et al., 2021), and 4426 ± 65 Ma (Premo and Tatsumoto, 1991) have also been determined. If all these ages are combined with Pb-Pb SIMS ages presented here a weighted average for 78235/6/8/55/56 is 4334.7 ± 3.5 Ma (MSWD = 3.3). Notably, the MSWD decreases to 0.33 if only the 7 most concordant ages are used in the weighted average remains the same (4334.1 ± 3.5 Ma). The concordance of the majority of the measured ages, combined with the relatively small uncertainty of the weighted average, suggests that the weighted average provides the best age estimate for the crystallization of norite 78235/6/8/55/56. This is our preferred age for the family of related norite samples 78235/6/8/55/56.

There have been two chronologic investigations of 60025 that have yielded different ages. The initial investigation by Carlson and Lugmair (1981) obtained an age of 4437 ± 39 Ma. A second study by Borg et al. (2011), redetermined the age of 60025 taking advantage of a sample with anomalously abundant and large (up to 1 cm) pyroxene grains. Three isotopic systems including ^{207}Pb-^{206}Pb (4359.2 ± 2.4 Ma), ^{147}Sm-^{143}Nd (4367 ± 11 Ma), and ^{146}Sm-^{142}Nd ($4350\ ^{+26}/_{-33}$ Ma; recalculated using t½(^{146}Sm) = 92 Ma of Chiera et al., 2024) were applied to the rock and yielded a weighted average age of 4359.5 ± 2.3 Ma. The concordance of the three ages combined with initial ε^{143}Nd values near 0 led the authors to the conclusion that this age recorded crystallization of 60025.

5.2 Cooling history

The isotopic systematics and measured ages of plutonic rocks, such as those investigated here, can be affected by the rate at which they cooled (e.g., Ganguly et al., 1998; McCallum and Schwartz, 2001; Borg et al., 2017). This reflects subsolidus diffusion that results in exchange of parent and daughter isotopes between mineral phases. The magnitude of elemental exchange is

480 dependent on the extent to which individual elements diffuse in specific minerals, the size of the
481 minerals (effective diffusion radius), the cooling rate, and the temperature of the rock (e.g.,
482 Dodson, 1973; Ganguly and Tirone, 1999). Generally speaking, the Rb-Sr, Sm-Nd, and U-Pb
483 isotopic systems are not affected once the temperature of the rock gets below about 850 °C (Borg
484 et al., 2017).

485 Cooling rates have been estimated in plutonic lunar samples from the width of pyroxene
486 exsolution lamellae. Using a QMD sample from 15403 McCallum and O'Brien (1996) estimated
487 a very rapid cooling rate of 0.2 °C/year. Our sample has pyroxene exsolution lamellae that are
488 similar in width to those described by McCallum and O'Brien (1996), implying that the measured
489 ages of Clast B closely reflect the time of emplacement and crystallization. The cooling history of
490 78235/6/8/55/56 is more complex than QMD Clast B. The absence of pyroxene exsolution
491 lamellae led Takeda et al. (1981) to suggest that the sample cooled slowly from a temperature
492 above the orthopyroxene-augite solvus until it reached a temperature slightly above 1000 °C at
493 which time it cooled rapidly. The conclusion that the exsolution temperature for pyroxene is within
494 a few hundred degrees of its solidus temperature of <1300 °C (Shearer et al., 2015) implies that
495 the measured ages of 78235/6/8/55/56 reasonably approximate the time of crystallization given
496 the rapid cooling rates estimated for similar Apollo 17 Mg-suite gabbronorites (McCallum and
497 O'Brien, 1996).

498 The cooling rate for 60025 is estimated by McCallum and O'Brien (1996) to be about 18
499 °C/Ma. Assuming an emplacement temperature near the solidus of ~1125 °C and a closure of the
500 Sm-Nd system at 870 °C, Borg et al. (2017) estimated the emplacement age of 60025 was ~16
501 Ma earlier than the crystallization age. Thus, the solidification of 60025 in the lunar crust may
502 have occurred as early as 4375 Ma, not 4359 ± 2.3 Ma recorded by the weighted average U-Pb

503 and Sm-Nd ages. Note that this calculation assumes that cooling is linear at a rate of 18 °C/Ma.
504 Given cooling is not expected to be linear, 4375 ± 2.3 Ma is the maximum crystallization age for
505 60025.

506 **5.3 Extent to which high precision ages represent duration of crustal magmatism**

507 The ages measured here and by Borg et al. (2011) are significantly more precise than
508 previous age determinations on lunar crustal rock samples (Borg et al., 2015; Papike et al., 2018;
509 Carlson and Borg, 2022), suggesting that several distinct styles of lunar magmatism are
510 contemporaneous within a few tens of millions of years. The observation that the age of the FAS
511 sample is about 25 Ma to at most 45 Ma older than the AKS and the MGS samples is consistent
512 with the temporal predictions for crustal magmatism based on the LMO model of lunar
513 differentiation in which FAS represents primary LMO cumulates and MGS and AKS represent
514 KREEP-rich secondary crustal rock suites. It is unclear, however, how representative these ages
515 are of the broader crustal rock suites.

516 If all measured ages reported in the literature over the last ~50 years are considered
517 equally, magmatism associated with the three suites of crustal lithologies must be
518 contemporaneous over several hundred million years (Figure 2) and some of the basic tenants of
519 the LMO model of differentiation would be incorrect. Importantly, many of the reported ages are
520 simply erroneous or do not record igneous crystallization as demonstrated by the fact that
521 multiple ages determined on single samples are often discordant (Figure 2). Thus, the
522 distribution of reported ages is likely to be a very poor representation of the duration of
523 magmatic activity associated with the three lunar crustal rock suites. Ages that are more
524 representative of the duration of magmatism associated with the FAS and MGS magmatic rock
525 suites may be obtained from whole rock Sm-Nd isochrons. These are model ages because they

assume that all of the samples are derived from a common source region at a common point in time. This is probably not too unrealistic given the observation that most Sm-Nd internal isochron measurements indicate these rocks are derived from sources with nearly identical initial Sm-Nd isotopic systematics (Borg et al., 2015). The benefit of this approach is that these Sm-Nd model ages are not affected by secondary disturbances, such as impact metamorphism or slow cooling, provided the Sm-Nd system remains closed in the whole rocks during the disturbance. The Sm-Nd system is ideal for this because both elements are refractory and behave almost identically during geochemical processing.

Eight MGS samples from the Apollo 14, 15, 16, and 17 sites that have been analyzed for Sm-Nd using the same analytical procedures, including ^{149}Sm-^{150}Nd tracer and neutron capture corrections, define a single whole rock isochron with an age corresponding to 4348 ± 25 Ma and an initial ε^{143}Nd value of -0.25 ± 0.09 with a MSWD = 1.4 (Borg et al., 2020). The collinearity of the Sm-Nd data implies that the various troctolites, norites, and gabbro norites included in this data set are derived from a source with a common initial ^{143}Nd/^{144}Nd ratio at a common point in time. The Sm-Nd isotopic data measured on six FAS samples using the same analytical procedures define a line on an isochron plot corresponding to an age of 4354 ± 29 Ma with an initial an initial ε^{143}Nd value of -0.39 ± 0.20 with a MSWD = 20 (Figure 9). Note that the regression yields a relatively large MSWD, underscoring the fact that Sm-Nd measurements on FAS samples are difficult as a result of the low abundances of REE and the typically large corrections on both their ^{147}Sm/^{144}Nd and the ^{143}Nd/^{144}Nd ratios due to substantial exposure to thermal neutrons. Nevertheless, internal isochron measurements made on three FAS samples analyzed using the same techniques are consistent, yielding ages of 4367 ± 11 Ma with an ε^{143}Nd value of -0.25± 0.09 for 60025 (Borg et al., 2011); 4350 ± 73 Ma with an initial ε^{143}Nd value of -

549 0.53 ± 0.26 for 62237 (Sio et al., 2020), and 4302 ± 28 Ma with an initial ε^{143}Nd value of -0.28 ±
550 0.14 for 60016 (Marks et al., 2019). Thus, although not definitive, the Sm-Nd isotope
551 systematics of FAS samples from the Apollo 15 and 16 sites, like the MGS samples, are
552 consistent with production of the FAS over a limited duration from a common source.

553 Igneous rocks of the AKS are rare and, with the exception of the QMD clasts in 15405,
554 have not yielded igneous crystallization ages. The only other AKS rock sample that has been
555 dated is "alkali-anorthosite" Clast B from 14304. Concordant Sm-Nd (3947±13 Ma), Rb-Sr
556 (3975±34 Ma) and Ar-Ar (3937±37 Ma) ages determined on this sample suggest, however, that it
557 is an impact melt produced during the formation of the Imbrium basin (Kruijer et al., 2023). The
558 QMD lithology is the only igneous rock type observed in either the Apollo or meteorite
559 collections that contains significant amounts of zircon, leading to the hypothesis that detrital
560 zircons found in impact melt breccias might, at least in part, represent additional ages of the
561 QMD lithology. The ages determined for detrital zircons from the Apollo 12, 14, 15, and 17
562 landing sites range in age from about 3.85 to 4.45 Ga and define a peak on a frequency
563 distribution diagram of 4340 ± 20 Ma (e.g., Grange et al., 2009; 2011; 2013; Meyer et al., 1996;
564 Nemchin et al., 2008; Nemchin et al., 2006; Nemchin et al., 2009a; Nemchin et al., 2009b;
565 Nemchin et al., 2012; Pidgeon et al., 2007, Borg et al., 2015; Barboni et al., 2024).

566 Although the whole rock isochrons and the age frequency distribution of detrital zircons
567 seems to provide more tightly constrained age ranges for FAS (4354 ± 29 Ma), MGS (4348 ± 25
568 Ma) and AKS (4340 ± 20 Ma) compared to the range of ages reported in the literature (Figure 2),
569 all three of these ages still overlap (Figure 10), underscoring the short time spans that separate
570 these magmatic events relative to the analytical uncertainties associated with the ages.
571 Nevertheless, high-precision ages obtained here suggest that the duration of magmatic activity

may be much more tightly compressed compared to the durations inferred from both the broader chronologic data set compiled for these rock suites (Figure 2) and the whole rock isochrons and age frequency distribution of detrital zircons (Figure 10).

If the high precision ages determined on FAS, MGS, and AKS samples presented here are representative of the broader rock suites then they constrain the timing of igneous crustal magmatic events responsible for the production of the lunar crust. This possibility is explored below. We emphasize that we are not implying that all magmatism associated with these suites is confined to the uncertainty associated with the age determinations on the FAS, MGS, and AKS samples. Instead, we are suggesting that these ages are the most reasonable representation of the age relationships among the three suites of crustal rocks that we currently have and, as such, are used to elucidate potential temporal and petrogenetic relationships.

5.4 Relationships among crustal rock suites

If the high precision ages of the three crustal samples discussed here are representative of the relationships among the broader rock suites, they imply that FAS magmatism proceeds MGS and AKS magmatism by about 35 ± 10 Ma. This is consistent with production of the lunar crust in the context of the magma ocean model of lunar differentiation in which plagioclase-rich primary FAS cumulates predate KREEP-rich MGS and AKS rocks. Furthermore, despite crystallization at distant landing sites, the ages of MGS norite samples 78235/6/8/55/56 and AKS sample 15405 Clast B are nearly identical (Figure 10), requiring widespread, compositionally distinct and contemporaneous, crustal magmatism around 4.34 Ga. Their chronologic relationship suggests that the heating mechanisms associated with the production of the MGS and AKS were probably the same. Given the likely limited duration of MGS and AKS magmatism, implied by the MGS whole rock Sm-Nd isochron and the peak in detrital zircon

595 ages, respectively, the heating event is also probably of short duration. Long-duration heating
596 mechanisms, such as decay of ^{238}U, ^{235}U, ^{232}Th, and ^{40}K, therefore seem unlikely. Melting due to
597 impact also seems unlikely because some of the MGS rocks, such as troctolite 76535, are
598 thought to have crystallized deep in the lunar crust or upper mantle (e.g., Gooley et al., 1974;
599 Dymek et al. 1975; McCallum and O'Brien, 1996; McCallum and Schwartz, 2001) beyond the
600 depth at which even very large impacts are likely to initiate melting. There are two scenarios
601 that can account for an episodic pulse of magmatism in the lunar crust and mantle. The first is
602 adiabatic melting associated with density driven overturn of the LMO cumulate pile (e.g., Taylor,
603 2009; Shearer et al., 2015; Prissel et al., 2023). The second is tidal heating associated with
604 gravitational interactions between the early Earth and Moon (Nimmo et al., 2024). Both heating
605 mechanisms are consistent with the chronologic measurements presented here and have the
606 potential to have produced the MGS and AKS.

607 The petrogenetic relationship between the MGS and the AKS is not clear. For instance,
608 some studies have claimed that MGS and the AKS might derive from distinct parental melts
609 (Warren and Wasson 1980; James 1980; James et al. 1987; Snyder et al., 1995a), whereas others
610 have suggested that they share a common set of parental magmas (Snyder et al., 1995b; Shervais
611 and McGee, 1999). The nearly perfect concordance between the age of the MGS norite
612 78235/6/8/55/56 and AKS 15405 QMD Clast B, as well as the concordance between the peak in
613 detrital zircon ages and the MGS whole rock isochron, strengthens the suggestion that the two
614 rock suites are related. Additional support for a potential petrogenetic relationship is based on
615 the observation that the initial $\varepsilon^{143}Nd$ isotopic composition of the QMD Clast B (-0.23 ± 0.11) is
616 the same as that measured for both the MGS norite 78238 (-0.27 ± 0.74) and the MGS whole
617 rock isochron at (-0.25 ± 0.09). The identical initial $\varepsilon^{143}Nd$ isotopic composition of MGS and

AKS requires their source materials to have identical time-averaged REE elemental systematics since the beginning of the Solar System. This is important because it means that if the MGS and the AKS are related, it must be through a closed system process such as fractional crystallization or partial melting. If these rocks were derived from different source materials, or assimilated isotopically distinct crustal rocks, or assimilated variable amounts of urKREEP during their evolution, their initial ε^{143}Nd values would almost certainly differ. Thus, relating the MGS to the AKS through fractional crystallization or partial melting of a common source appears to be the most reasonable explanation for the temporal and isotopic relationships determined here.

5.5 Temporal relationship between crustal and mantle cumulates

A model age for the crystallization of LMO mafic cumulates (mare basalt sources) is calculated from the slope of a ^{142}Nd/^{144}Nd versus ^{147}Sm/^{144}Nd isochron plot. The approach to estimating the age of crystallization of the LMO using this system was developed by Nyquist et al. (1995) and has been adopted by numerous authors (e.g., Rankenburg et al. 2006, Boyet & Carlson 2007, Brandon et al. 2009, McLeod et al. 2014, Borg et al. 2019), resulting in an average model age of 4348 ± 29 Ma (Borg and Carlson, 2022; uncertainty is 2 s.d.; MSWD = 9.2). These ages were calculated assuming the half-life of ^{146}Sm was 103 Ma. A more recent determination of half-life of ^{146}Sm of 92.0 ± 2.6 Ma (Chiera et al., 2024) changes the average model age for LMO crystallization substantially to 4376 ± 25 Ma. As in the previous calculation, the age uncertainty includes ~6 Ma contributed by the uncertainty associated with the decay constant. The ^{146}Sm-^{142}Nd isochron model age is concordant with the measured age of 60025 of 4359.3 ± 2.3 Ma as well as with the maximum estimated emplacement age of 4375.3 ± 2.3 Ma calculated assuming a linear cooling history at ~18 °C/Ma (McCallun and O'Brien, 1996) from 1125°C to 870°C (Borg et al., 2017). These ages suggest that mafic and felsic cumulates of the LMO

crystalized contemporaneously within uncertainty and that both crystallized about 30 to 40 Ma prior to the production of MGS and AKS magmas.

6. CONCLUSION

A summary of the temporal relations discussed here is presented in Figure 11. Multiple chronometric systems define weighted averages for FAS sample 60025, MGS norite 78235/6/8/55/56, and AKS QMD 15405 Clast B of 4359.3 ± 2.3 Ma (Borg et al., 2011; N=3), 4334.1 ± 3.5 Ma (N=7), and 4337.19 ± 0.49 Ma (N=4) respectively. The fact that these ages are defined by multiple concordant chronometers demonstrates that they record the time of crystallization of the samples. The weighted average ages determined on individual samples are concordant with less precise model Sm-Nd whole rock ages of FAS and MGS samples, as well as the peak of Pb-Pb ages defined for detrital zircons, that are probably petrologically associated with the AKS. This implies that all three suites of lunar crustal rocks formed over a very limited time interval of 25 to 45 Ma. Furthermore, FAS magmatism appears to be about 35 ± 10 Ma older than MGS and AKS magmatism which is consistent with temporal predictions from the LMO model of lunar differentiation. The MGS and AKS appear to be contemporaneous despite being present at widely spaced locations on the Moon. Similar initial Nd isotopic compositions of MGS and AKS further suggest that they are derived from similar sources sharing a common time averaged Sm/Nd ratio.

The age relationships defined here suggest that there were two distinct and widespread pulses of crust building on the Moon. The first was associated with primordial solidification of the Moon resulting in the production of FAS. The second magmatic pulse produced both the

MGS and AKS a few tens of millions of years later. It is only through high precision chronologic measurements that these events can be distinguished temporally. Although obtaining such high precision ages has been an objective of the lunar science community for many decades, much more work, and many more age determinations based on multiple concordant isotopic systems, are necessary to evaluate if the broad ramifications explored here are accurate. In addition to the analytical challenges discussed above, a major limitation associated with understanding the early evolution of the Moon is the extreme paucity of appropriate samples. As large and meaningful samples masses are likely to be returned from the Moon in the next few decades significant preparation is needed to ensure that enough of these very rare and extremely important highlands samples are obtained to address the fundamental questions of how and when the Moon formed.

Data Availability: Data available at https://data.mendeley.com/datasets/76jm6zrr3d/1

Acknowledgements: Funding from Laboratory Directed Research and Development Program at Lawrence Livermore National Laboratory (Grant 23-ERD-003) as well as NASA Emerging Worlds Program (Grant NNH19ZDA001N) is gratefully acknowledged. We are very thankful to Mark Schmitz (Boise State University) for providing an aliquot of the BSU1b ^{205}Pb-^{233}U-^{235}U tracer. We are grateful for constructive reviews from Dr. James Connely, Dr. Klaus Mezger, and an anonymous reviewer. This study was performed under the auspices of the US DOE by Lawrence Livermore National Laboratory under Contract DE-AC52-07NA27344 with release number LLNL-JRNL-2003346.

Appendix A. Supplementary Materials

This section contains analytical methods for electron microprobe analysis of minerals, elemental abundances measurements of mineral fractions, Rb-Sr and Sm-Nd isotopic analysis of mineral fractions, zircon U-Pb isotope dilution analysis, and zircon Pb-Pb *in Situ* isotope analysis. Zircon dissolution and chemical separation, U-Pb mass spectrometry, and accuracy and

689 reproducibility of U-Pb and Pb-Pb data are discussed. Supplementary data table included in the
690 supplement include: Table S1. Representative composition of minerals from 15405 QMD Clast
691 B, Table S2. Major and trace element abundances QMD Clast B mineral fractions, Table S3. U-Pb
692 isotope dilution Data for Temora zircon standards, and Table S4. Effect of varying Pb blank
693 contributions and compositions on $^{207}Pb/^{206}Pb$ ages of 15405 QMD Clast B zircons
694

7. REFERENCES

Barboni M., Szymanowski D., Schoene B., Dauphas N., Zhang Z. J., Chen X., and McKeegan K. D. (2024). High-precision U-Pb zircon dating identifies a major magmatic event on the Moon at 4.338 Ga. *Sci. Adv.* **10,** eadn9871.

Barboni M., Boehnke P., Keller B., Kohl I. E., Schoene B., Young E. D., and McKeegan K. D. (2017) Early formation of the Moon 4.51 billion years ago. *Sci. Adv.* **3,** e1602365.

Borg L. E. and Carlson R.W. (2022) The evolving chronology of moon formation. *An. Rev. Earth Planet. Sci.* **51,** 25–52.

Borg L. E., Connelly J. N., Boyet M., and Carlson R. W. (2011) Chronological evidence that the Moon is either young or did not have a global magma ocean. *Nat.* **477,** 70–72.

Borg L. E., Gaffney A. M., and Shearer C. K. (2015) A review of lunar chronology revealing a preponderance of 4.34–4.37 Ga ages. *Meteorit. Planet. Sci*. **50,** 715–732.

Borg L. E., Brennecka G. A., and Symes S. J. (2016). Accretion timescale and impact history of Mars deduced from the isotopic systematics of martian meteorites. *Geochim. Cosmochim. Acta* **175,** 150-167.

Borg L. E., Connelly J. N., Cassata W. S., Gaffney A. M., and Bizzarro M. (2017) Chronologic implications for slow cooling of troctolite 76535 and temporal relationships between the Mg-suite and the ferroan anorthosite suite. *Geochim. Cosmochim. Acta* **201,** 377–391.

Borg L. E., Gaffney A. M., Kruijer T. S., Marks N. A., Sio C. K., and Wimpenny J. (2019) Isotopic evidence for a young lunar magma ocean. *Earth Planet. Sci. Lett.* **523,** 115706.

Borg L. E., Cassata W. S., Wimpenny J., Gaffney A. M., and Shearer C. K. (2020) The formation and evolution of the Moon's crust inferred from the Sm-Nd isotopic systematics of highlands rocks. *Geochim. Cosmochim. Acta* **290,** 312–332.

Boyet M. and Carlson R.W. (2007) A highly depleted moon or a non-magma ocean origin for the lunar crust? *Earth Planet. Sci. Lett.* **262,** 505–516.

Boyet M., Carlson R. W., Borg L. E., and Horan M. (2015) Sm–Nd systematics of lunar ferroan anorthositic suite rocks: Constraints on lunar crust formation. *Geochim. Cosmochim. Acta* **148,** 203–218.

Brandon A. D., Lapen T. J., Debaille V., Beard B. L., Rankenbur, K., and Neal C. (2009) Reevaluating $^{142}Nd/^{144}Nd$ in lunar mare basalts with implications for the early evolution and bulk Sm/Nd of the Moon. *Geochim. Cosmochim. Acta* **73,** 6421–6445.

Carlson R. W. and Lugmair G. T. (1981). Time and duration of lunar highlands crust formation. *Earth Planet. Sci. Lett.* **52,** 227-238.

Chiera N. M., Sprung P., Amelin Y., Dressler R., Schumann D., and Talip Z. (2024). The 146 Sm half-life re-measured: consolidating the chronometer for events in the early Solar System. *Sci. Rep.* **14,** 17436.

Condon D. J., Schoene B., McLean N. M., Bowring S. A., and Parrish, R. R. (2015). Metrology and traceability of U–Pb isotope dilution geochronology (EARTHTIME Tracer Calibration Part I). *Geochim. Cosmochim. Acta* **164,** 464-480.

734 Dodson M. H. (1973). Closure temperature in cooling geochronological and petrological
735 systems. *Contrib. Min. Pet.* **40,** 259-274.

736 Drozd R. J., Kennedy B. M., Morgan C. J., Podosek F. A. and Taylor G. J. (1976) The excess
737 fission Xenon problem in lunar samples. *Proc. 7th Lunar Sci. Conf*. 599-623.

738 Dymek R. F., Albee A. L. and Chodos A. A. (1975) Comparative petrology of lunar cumulate
739 rocks of possible primary origin: Dunite 72415, troctolite 76535, norite 78235, and
740 anorthosite 62237. *Proc. 6th Lunar Sci. Conf.* 301-341.

741 Edmunson J., Borg L. E., Nyquist L. E., and Asmeron Y. (2009) A combined Sm–Nd, Rb–Sr, and
742 U-Pb isotopic study of Mg-suite norite 78238: Further evidence for early differentiation of
743 the Moon. *Geochim. Cosmochim. Acta* **73,** 514–527.

744 Elardo S. M., Draper D. S., and Shearer Jr C. K. (2011). Lunar Magma Ocean crystallization
745 revisited: Bulk composition, early cumulate mineralogy, and the source regions of the
746 highlands Mg-suite. *Geochim. Cosmochim. Acta* **75,** 3024-3045.

747 Elkins-Tanton L. T., Burgess S., and Yin Q. Z. (2011). The lunar magma ocean: Reconciling the
748 solidification process with lunar petrology and geochronology. *Earth Planet. Sci. Lett.* **304,**
749 326-336.

750 Fagan T. J., Kashima D., Wakabayashi Y., and Suginohara A. (2014). Case study of magmatic
751 differentiation trends on the Moon based on lunar meteorite Northwest Africa 773 and
752 comparison with Apollo 15 quartz monzodiorite. *Geochim. Cosmochim. Acta* **133,** 97-127.

753 Floss C., James O. B., McGee J. J., and Crozaz G. (1998) Lunar ferroan anorthosite petrogenesis:
754 Clues from trace distributions in FAN subgroups. *Geochim. Cosmochim. Acta* **62,** 1255-
755 1283.

756 Gaffney A. M., Borg L. E., Asmerom Y., Shearer C. K., and Burger P. V. (2011) Disturbance of
757 isotope systematics during experimental shock and thermal metamorphism of a lunar basalt
758 with implications for Martian meteorite chronology. *Meteorit. Planet. Sci.* **46,** 35-52.

759 Ganguly J. and Tirone M. (1999). Diffusion closure temperature and age of a mineral with
760 arbitrary extent of diffusion: theoretical formulation and applications. *Earth Planet. Sci. Lett.*
761 **170,** 131-140.

762 Ganguly J., Tirone M., and Hervig R. L. (1998) Diffusion kinetics of samarium and neodymium
763 in garnet, and a method for determining cooling rates of rocks. *Sci.* **281,** 805-807.

764 Gooley R. C., Brett R., Warner J. L., and Smyth J. R. (1974) A lunar rock of deep crustal origin:
765 Sample 76535. *Geochim. Cosmochim. Acta* **38,** 1329-1339.

766 Grange M. L., Nemchin A. A., Pidgeon R. T., Timms N., Muhling J. R., and Kennedy A .K.
767 (2009) Thermal history recorded by the Apollo 17 impact melt breccia 73217. *Geochim.*
768 *Cosmochim. Acta* **73,** 3093–3107.

769 Grange M. L., Nemchin A. A., Timms N., Pidgeon R. T., and Meyer C. (2011) Complex
770 magmatic and impact history prior to 4.1 Ga recorded in zircon from Apollo 17 South Massif
771 aphanitic breccia 73235. *Geochim. Cosmochim. Acta* **75,** 2213–2232.

772 Grange M. L., Pidgeon R. T., Nemchin A. A., Timms N. E., and Meyer C. (2013) Interpreting U-
773 Pb data from primary and secondary features in lunar zircon. *Geochim. Cosmochim. Acta*
774 **101,** 112–132.

775 Gros J., Takahashi H., Morgan J. W., and Anders E. (1976) Siderophile and volatile elements in
776 Apollo 14 and 15 rocks of the Imbrium Consortium. In Interdisciplinary studies by the
777 Imbrium Consortium. Volume 2. (J.A. Wood ed.) LSI contribution 268D Center for
778 Astrophysics, Cambridge.

779 Hinthorne J. R., Conrad R. L., and Church S. E. (1977) Lead-lead age and rare earth element
780 determinations in lunar norite 78235 (abs). Lunar Sci. **VIII,** 444-446. Lunar Planetary
781 Institute, Houston.

782 Jackson E. D., Sutton R. L. and Wilshire H. G. (1975) Structure and petrology of a cumulus
783 norite boulder sampled by Apollo 17 in Taurus-Littrow valley, the Moon. *Geol. Soc. Am.*
784 *Bull*. **86,** 433-442.

785 Jaffey A. H., Flynn K. F., Glendenin L. E., Bentley W. T., and Essling A. M. (1971) Precision
786 measurement of half-lives and specific activities of U 235 and U 238. *Phy. Rev. C* **4,** p. 1889.

787 James O. B. (1980) Rocks of the early lunar crust. *Proc. 11th Lunar Planet. Sci. Conf.* 365–393.

788 James O. B., Lindstrom M. M., and Flohr M. K. (1987) Petrology and geochemistry of alkali
789 abbronorites from lunar breccia 67975. *Proc. 17th Lunar Sci. Conf*. E314–E330. Lunar
790 Planetary Institute, Houston.

791 James O. B., Lindstrom M. M., and McGee J. J. (1991) Lunar ferroan anorthosite 60025:
792 Petrology and chemistry of mafic lithologies. *Proc. 21st Lunar Planet. Sci. Conf.* 63-87.
793 Lunar Planetary Institute, Houston.

794 Joy K. H., Wang N., Snape J. F., Goodwin A., Pernet-Fisher J. F., Whitehouse M. J., Liu Y., Lin
795 Y. T., Darling J. R., Tar P., and Tartese R. (2025) Evidence of a 4.33 billion year age for the
796 Moon's South Pole–Aitken basin. *Nat. Astro*. **9,** 55-65.

797 Jolliff B. L. (1991) Fragments of quartz monzodiorite and felsite in Apollo 14 soil particles.
798 *Proc. 21st Lunar Planet. Sci. Conf.* 101-118. Lunar Planetary Institute, Houston.

799 Krogh T. E. (1973) A low contamination method for hydrothermal decomposition of zircon and
800 extraction of U and Pb for isotopic age determination. *Geochim. Cosmochim. Acta* **37,** 485–
801 494.

802 Kruijer T. S., Borg L. E., Cassata W. S., Wimpenny J., Brennecka G. A., Shearer C. K., and
803 Simon S. B. (2023) Chronology of alkali anorthosite 14304 clast "b" records basin forming
804 impact at ~3.95 Ga. *Geochim. Cosmochim. Acta* **358,** 61-76.

805 Lin Y., Tronche E. J., Steenstra E. S., and van Westrenen W. (2017) Evidence for an early wet
806 Moon from experimental crystallization of the lunar magma ocean. *Nat. Geo*. **10,** 14-18.

807

808 Marks N. E., Borg L. E., Shearer C. K., and Cassata W. S. (2019) Geochronology of an Apollo
809 16 clast provides evidence for a basin-forming impact 4.3 billion years ago. *J. Geophys. Res.*
810 *Planet* **124,** 2465-2481.

811 Marvin U. B., Lindstrom M. M., Holmberg B. B. and Martinez R. R. (1991) New observations of
812 quartz monozodiorite granite suite. *Proc. 21st Lunar Planet. Sci. Conf.* 119-136. Lunar
813 Planetary Institute, Houston.

814 Mattinson J. M. (2005) Zircon U–Pb chemical-abrasion ("CA-TIMS") method: Combined
815 annealing and multi-step dissolution analysis for improved precision and accuracy of zircon
816 ages. *Chem. Geo.* **220,** 47–56.

817 McCallum I. S. and Mathez E. A. (1975) Petrology of noritic cumulates and a partial melting
818 model for the genesis of Fra Mauro basalts. *Proc. 6th Lunar Sci. Conf.* 395-414. Lunar
819 Planetary Institute, Houston.

820 McCallum I. S. and O'Brien H. E. (1996) Stratigraphy of the lunar highland crust: Depths of
821 burial of lunar samples from cooling-rate studies. *Am. Min*. **81,** 1166-1175.

822 McCallum I. S. and Schwartz J. M. (2001) Lunar Mg suite: Thermobarometry and petrogenesis
823 of parental magmas. *J. Geophys. Res. Planet* **106,** 27969-27983.

824 McLean, N.M., Bowring, S.A., Grove, M., de Oliveira, E.P., Condon, D.J., 2015. Evaluating
825 uncertainties in the calibration of isotopic reference materials and multi-element isotopic
826 tracers (EARTHTIME Tracer Calibration Part II). Geochimica et Cosmochimica Acta 164,
827 481-501.

828 McLeod C., Brandon A. D., and Armytage R. M. G. (2014) Constraints in the formation age and
829 evolution of the Moon from ^{142}Nd-^{143}Nd systematics of Apollo 12 basalts. *Earth Planet. Sci.*
830 *Lett.* **396,** 179–189.

831 Meissner F., Schmidt-Ott W -D., and Ziegeler L. (1987) Half-life and α-ray energy of ^{146}Sm.
832 *Zeitschrift für Physik A Atomic Nuclei* **327,** 171-174.

833 Meyer C. (1994) Catalog of Apollo 17 rocks. Curator's Office JSC, 26088, 644.

834 Meyer C., Williams I. S., and Compston W. (1996) Uranium-lead ages for lunar zircons:
835 Evidence for a prolonged period of granophyre formation from 4.32 to 3.88 Ga. *Meteorit.*
836 *Planet. Sci.* **31,** 370–387.

837 Mundil R., Ludwig K.R., Metcalfe I., and Renne P. R. (2004) Age and timing of the Permian
838 mass extinctions: U/Pb dating of closed-system zircons. *Sci.* **305,** 1760–1763.

839 Nakamura N., Masuda A., Tanaka T. and Kurasawa H. (1973) Chemical compositions and rare-
840 earth features of four Apollo 16 samples. *Proc. 4th Lunar Sci. Conf.* 1407-1414.

841 Nemchin A. A., Grange M. L., Pidgeon R. T., and Meyer C. (2012) Lunar zirconology. Austral.
842 *J. Earth Sci*. **59,** 277-290.

843 Nemchin A. A., Whitehouse M. J., Pidgeon R. T., and Meyer C. (2006) Oxygen isotopic
844 signature of 4.4–3.9 Ga zircons as a monitor of differentiation processes on the Moon.
845 *Geochim. Cosmochim. Acta* **70,** 1864–1872.

Nemchin A. A., Pidgeon R. T., Whitehouse M. J., Vaughan J. P., and Meyer C. (2008) SIMS U-Pb study of zircon from Apollo 14 and 17 breccias: Implications for the evolution of lunar KREEP. *Geochim. Cosmochim. Acta* **72,** 668–689.

Nemchin A., Timms N., Pidgeon R., Geisler T., Reddy S., and Meyer C. (2009a) Timing of crystallization of the lunar magma ocean constrained by the oldest zircon. *Nat. Geosci*. **2,** 133–136.

Nemchin A. A., Pidgeon R. T., Healy D., Grange M. L., Whitehouse M.J., and Vaughan J. (2009b) The comparative behavior of apatite-zircon U-Pb systems in Apollo 14 breccias: Implications for the thermal history of the Fra Mauro Formation. *Meteorit. Planet. Sci*. **44,** 1717–1734.

Nemchin A. A., Long T., Jolliff B .L., Wan Y., Snape J.F., Zeigler,R., Grange M. L., Liu D., Whitehouse M. J., Timms N. E., and Jourdan F. (2021) Ages of lunar impact breccias: Limits for timing of the Imbrium impact. *Geochem.* **81,** 125683.

Nimmo F., Kleine T., and Morbidelli A. (2024) Tidally driven remelting around 4.35 billion years ago indicates the Moon is old. *Nat.*, **636,** 598-602.

Norman M. D., Duncan R. A., and Huard J. J. (2006) Identifying impact events within the lunar cataclysm from ^{40}Ar–^{39}Ar ages and compositions of Apollo 16 impact melt rocks. *Geochim. Cosmochim. Acta* **70,** 6032–6049.

Nyquist L. E., Bansal B. M, and Wiesmann H. (1976a) Rb-Sr analysis of 15405, 87. Interdisciplinary Studies by the Imbrium Consortium 1 Eds. J.A. Wood. LPI contribution 267D. 97-101.

Nyquist L. E., Wiesmann H., Shih C. -Y., and Bansal. B. M. (1976b) 15405 Quartz-Monzodiorite: Super KREEP. Interdisciplinary Studies by the Imbrium Consortium 2. Eds. G. Ryder, U.B. Marvin, J.F. Bower, K. Motylewski, and J.A. Wood. LPI contribution 268. 30-41.

Nyquist L. E., Reimold W. U., Bogard D.D., Wooden J. L., Bansal B. M., Wiesmann H., and Shih C.-Y. (1981) A comparative Rb-Sr, Sm-Nd and K-Ar study of shocked norite 78236: Evidence of slow cooling in the lunar crust? *Proc. 12th Lunar Planet. Sci. Conf*. 67-97. Lunar Planetary Institute, Houston.

Nyquist L. E., Hörz F., Wiesmann H., Shih C.-Y., and Bansal B. (1987) Isotopic studies of shergottite chronology: I. effect of shock metamorphism on the Rb–Sr system. Lunar Planet. Inst. Conf. Abst. 732–733.

Nyquist L. E., Wiesmann H., Bansal B. M., Shih C.-Y., Keith J. E., Harper C. L. (1995) ^{146}Sm-^{142}Nd formation interval for the lunar mantle. *Geochim. Cosmochim. Acta*. **59,** 2817–2837.

Papike J. J., Ryder G., and Shearer C. K. (2018) Chapter 5. LUNAR SAMPLES. In: Papike, J.J. (Ed.), Planetary Materials. De Gruyter, pp. 719–952.

Pidgeon R. T., Nemchin A. A., Van Bronswijk W., Geisler T., Meyer C., Compston W., and Williams I. S. (2007) Complex history of a zircon aggregate from lunar breccia 73235. *Geochim. Cosmochim. Acta,* **71,** 1370-1381.

885 Premo W. R. and Tatsumoto M. (1991) U-Th-Pb isotopic systematics of lunar norite 78235.
886 *Proc. 21st Lunar Planet. Sci. Conf.* 89-100. Lunar Planetary Institute, Houston.

887 Premo W. R., Tatsumoto M., Misawa K., Nakamura N., and Kita N. I. (1999) Pb-isotopic
888 systematics of lunar highland rocks (> 3.9 Ga): constraints on early lunar evolution. *Int. Geo.*
889 *Rev*.**41**, 95-128.

890 Prissel T. C., Zhang N., Jackson C. R., and Li H. (2023) Rapid transition from primary to
891 secondary crust building on the Moon explained by mantle overturn. *Nat. Comm*.**14,** 5002.

892 Rankenburg K., Brandon A. D., and Neal C. R. (2006) Neodymium isotope evidence for
893 chondritic composition of the Moon. *Sci.* **312,** 1369–1372.

894 Rapp J. F. and Draper D. S. (2018) Fractional crystallization of the lunar magma ocean: Updating
895 the dominant paradigm. *Meteorit. Planet. Sci*. **53,** 1432-1455.

896 Ryder G. (1976). Lunar sample 15405: Remnant of a KREEP basalt-granite differentiated
897 pluton. *Earth Planet. Sci. Lett.* 29, 255-268.

898 Ryder G. (1982) Lunar anorthosite 60025, the petrogenesis of lunar anorthosites and the
899 composition of the Moon. *Geochim. Cosmochim. Acta* **46,** 1591-1601.

900 Ryder G. and Wood J. A. (1976) Samples 14064, 14082, 14312, 14318, 15405, and 15445 (with
901 a comparative petrological survey of 15455). In Interdisciplinary studies by the Imbrium
902 Consortium. Volume 2. J.A. Wood ed.) LSI contribution 268D Center for Astrophysics,
903 Cambridge.

904 Ryder G. and Bower J. F. (1976) Petrology. In Interdisciplinary studies by the Imbrium
905 Consortium. Volume 2. J.A. Wood ed.) LSI contribution 268D Center for Astrophysics,
906 Cambridge.

907 Ryder G. and Norman M. D. (1979) Catalog of pristine non-mare materials Part 1. Non-
908 anorthosites, revised. NASA-JSC Curatorial Facility Publ. JSC 14565, Houston. 147 pp.

909 Ryder G. and Martinez R. R. (1991) Evolved hypabyssal rocks from station 7, Apennine Front,
910 Apollo 15. *Proc. 21st Lunar Planet. Sci. Conf.* 137-150. Lunar and Planetary Institute.

911 Sclar C. B. and Bauer J. F. (1975) Shock-induced subsolidus reduction-decomposition of
912 orthopyroxene and shock induced melting of norite 78235. *Proc. 6th Lunar Sci. Conf.* 799-
913 820.

914 Sclar C. B. and Bauer J. F. (1976a) Subsolidus reduction phenomena in lunar norite 78235:
915 Observations and interpretations. *Proc. 7th Lunar Sci. Conf.* 2493-2508.

916 Shearer C. K., Hess P. C., Wieczorek M. A., Pritchard M. E., Parmentier E. M., Borg L. E.,
917 Longhi J., Elkins-Tanton L. T., Neal C. R., Antonenko I., Canup R. M., Halliday A. N.,
918 Grove T. L., Hager B.H., Lee D.-C., Wiechert U. (2006) Thermal and magmatic evolution of
919 the Moon. *Rev. Min. Geochem*. **60,** 365–518.

920 Shearer C. K., Elardo S. M., Petro N. E., Borg L. E., McCubbin F. M. (2015) Origin of the lunar
921 highlands Mg-suite: An integrated petrology, geochemistry, chronology, and remote sensing
922 perspective. *Am. Mineral*. **100,** 294–325.

Shervais J. W. and McGee J. J. (1999) KREEP cumulates in the western lunar highlands; ion and electron microprobe study of alkali-suite anorthosites and norites from Apollo 12 and 14. *Am. Mineral.* **84,** 806–820.

Sio C. K., Borg L. E., and Cassata W. S. (2020) The timing of lunar solidification and mantle overturn recorded in ferroan anorthosite 62237. *Earth Planet. Sci. Lett*. **538,** 116219.

Smith J. V. and Steele I. M. (1974) Intergrowths in lunar and terrestrial anorthosites with implications for lunar differentiation. *Am Min.: J. Earth Planet. Materials* **59,** 673-680.

Snape J. F., Nemchin A. A., Grange M. L., Bellucci J. J., Thiessen F., and Whitehouse M.J. (2016) Phosphate ages in Apollo 14 breccias: Resolving multiple impact events with high precision U-Pb SIMS analyses. *Geochim. Cosmochim. Acta* **174,** 13–29.

Snyder G. A., Taylor L. A., and Neal C. R. (1992) A chemical model for generating the source of mare basalts: Combined equilibrium and fractional crystallization of the lunar magmashpere. *Geochim. Cosmochim. Acta* **56,** 3809–3823.

Snyder G. A., Taylor L. A., and Halliday A. N. (1995a) Chronology and petrogenesis of the lunar highlands alkali suite: Cumulates from KREEP basalt crystallization. *Geochim. Cosmochim. Acta* **59,** 1185-1203.

Snyder G.A., Neal C.R., Taylor L.A., and Halliday A.N. (1995b) Processes involved in the formation of the magnesian-suite plutonic rocks from the highlands of the Earth's Moon. *J. Geophys. Res. Planet.* **100,** 9365–9388.

Stacey J. T. and Kramers J. D. (1975). Approximation of terrestrial lead isotope evolution by a two-stage model. *Earth Planet. Sci. Lett.* **26,** 207-221.

Steele I. M. (1975) Mineralogy of lunar norite 78235: Second lunar occurrence of P21ca pyroxenes from Apollo 17 soils. *Am. Min*. **60,** 1086-1091.

Streckeisen A. (1976). To each plutonic rock its proper name. *Earth Sci. Rev.* **12,** 1-33.

Takeda H., Mori H., Ishii T. and Miyamoto M. (1981) Thermal and impact histories of pyroxenes in lunar eucrite like gabbros and eucrites. *Proc. 12th Lunar Planet. Sci. Conf.* 1297-1313.

Taylor G. J., Warner R. D., Keil K., Ma M.-S., and Schmitt R. A. (1980) Silicate liquid immiscibility, evolved lunar rocks, and the formation of KREEP. *In Proc. Conf. Lunar Highlands Crust, Geochim. Cosmochim. Acta Suppl*. **12.** Pergamon Press. 339-352. Lunar Planetary Institute, Houston.

Taylor G. J. (2009) Ancient Lunar Crust: Origin, Composition, and Implications. *Elements* **5,** 17-22.

Tera F. and Wasserburg G. J. (1972) U-Th-Pb systematics in lunar highland samples from the Luna 20 and Apollo 16 missions. *Earth Planet. Sci. Lett.* **17,** 36-51.

Walker D., Longhi J., and Hays J. F. (1975) Differentiation of a very thick magma body and implications for the source regions of mare basalts. *Proc. 6th Lunar Sci. Conf.* 1103-1120.

Warren P. H. (1985) The magma ocean concept and lunar evolution. *An. Rev. Earth Planet. Sci.* **13,** 201-240.

961 Warren P. H. (1993) A concise compilation of petrologic information on possibly pristine
962 nonmare Moon rocks. *Am. Min.* **78,** 360-376.

963 Warren P. H. and Wasson J. T. (1979) The origin of KREEP. *Rev. Geophys.* **17**, 73-88.

964 Warren P. H. and Wasson J. T. (1980) Further foraging for pristine nonmare rocks: Correlations
965 between geochemistry and longitude. *Proc. 11th Lunar Planet. Sci. Conf.* 431–470.

966 Warren P.H., Jerde E.A., and Kallemeyn G.W. (1987) Pristine moon rocks: A large felsite and a
967 metal-rich ferroan anorthosite. Proc. 17th Lunar Planet. Sci. Conf. in *J. Geophys. Res*. **90,**
968 E303-E313.

969 Wood J. A., Dickey J. S., Marvin U. B., and Powell B. N. (1970) Lunar anorthosites and a
970 geophysical model of the Moon. *Proc. 11th Lunar Planet. Sci. Conf.* 965–988.

971 Zhang B., Lin Y., Moser D. E., Warren P. H., Hao J., Barker I. R., Shieh S. R. Bouvier A. (2021)
972 Timing of lunar Mg-suite magmatism constrained by SIMS U-Pb dating of Apollo norite
973 78238. *Earth Planet. Sci. Lett*. **569,** 117046.

974
975

Figure captions

Figure 1. Cartoon cross section of lunar crust and upper mantle depicting temporal relationships between FAS, MGS, and AKS based on petrologic relationships between the rock suites. Samples enriched in the late stage LMO crystallization product KREEP are expected to be younger than primordial crystallization products of the LMO such as the FAS. The petrologic relationship between the MGS and AKS is uncertain, so these rock suites are depicted as both derived from independent sources (left side of cartoon) and related through magmatic evolution (center of cartoon).

Figure 2. Histogram of lunar crustal rock and detrital zircon ages. Data summarized from Borg et al. (2015), Papike et al (2018) and Borg and Carlson (2022). Zircon data for 72255 represented by open bar with preferred age in black (Zhang et al., 2021).

Figure 3. Backscatter Electron Image (BSE) of QMD Clast B fragment 4. Px = pyroxene, Plag = plagioclase, K-Feld = K-Feldspar, Qtz = quartz.

Figure 4. Rare earth element patterns of 15405 QMD Clast B, 15405 QMD Clast A, 78236/8 MGS norite, and 60025 FAS ferroan anorthosite. Data from Nakamura et al. (1973), Warren et al., (1987), Nyquist et al. (1976a, 1976b), Ryder (1976), Taylor et al. (1980), Borg et al. (2019), and this study.

Figure 5. Pb-Pb ages of zircons from QMD 15405 Clast B and baddeleyites from norite 78236/55. Uncertainties on all weighted averages are 2σ.

Figure 6: U-Pb concordia diagram for the zircons from 15405 QMD Clast B analyzed in this study. Displayed are zircon residue (R) fractions used in age calculations (blue ellipses), as well as R and L2 fractions omitted from age calculations (red ellipses). Discordia (solid black line) and associated upper and lower intercept values were calculated through linear regression of five R fractions. The inset provides a magnified view of the same diagram, emphasizing zircons that plot near the upper intercept value.

Figure 7. Sm-Nd isochron diagrams for 15405 QMD Clast B. A. 147Sm-143Nd isochron plot, B. 146Nd-142Nd isochron plot, C. 143Nd/144Nd-142Nd/144Nd isochron plot. Half life of 146Sm used in calculations is 92 Ma (Chiera et al., 2024).

Figure 8. Rb-Sr isochron diagram of QMD Clast A (Blue squares; Nyquist et al., 1976a, 1976b) and QMD Clast B (Red circles; this study) from 15405. Reference line is calculated assuming a bulk Moon 87Sr/86Sr at 4337 Ma of 0.69905.

Figure 9. FAS whole rock Sm-Nd isochron plot. Data from Boyet et al., 2015; Sio et al., 2020; Borg et al., 2011; Marks et al., 2019.

Figure 10. Summary of ages for sample suites (colored bars) based on whole rock isochrons or frequency of detrital zircon ages. Highest precision ages completed on individual AKS and MGS (this study), as well as FAS samples (Borg et al. 2011) are represented by black bars. Arrow on 60025 age represents maximum age of emplacement after accounting for delayed closure of the Sm-Nd system due to slow cooling in the crust (see text).

Figure 11. Cartoon cross section of lunar crust and upper mantle depicting temporal relationships between FAS, MGS, and AKS based on chronology presented here. Symbols same as figure 1.

Table 1. U-Pb isotope dilution data for 15405 QMD Clast B zircon residue (R) and leachate (L) fractions.

Sample	Dates (Ma)							Composition				Isotopic Ratios								
	$^{206}Pb/^{238}U$ <Th>[a,b]	±2σ abs	$^{207}Pb/^{235}U$	±2σ abs	$^{207}Pb/^{206}Pb$	±2σ abs	% disc[c]	Pb* (pg) [d]	Pbc (pg) [e]	Pb*/ Pbc [f]	Th/U (Min)	$^{206}Pb/^{204}Pb$ [h]	$^{208}Pb/^{206}Pb$ [i]	$^{206}Pb/^{238}U$ <Th> [i,a]	±2σ %	$^{207}Pb/^{235}U$ [i]	±2σ %	$^{207}Pb/^{206}Pb$ <Th> [i,a]	±2σ %	Corr. Coef.
ZR-1 (R)	4315.2	4.0	4330.3	1.9	4337.3	1.4	0.51	88.1	1.65	53.44	0.39	2398	0.10	0.9531	0.13	70.14	0.19	0.53400	0.089	0.91
ZR-4 (R)	4098	37	4259	12	4336.0	2.7	5.5	28.4	1.08	26.40	0.42	1188	0.11	0.888	1.2	65.31	1.2	0.53353	0.18	0.99
ZR-5 (R)	4273	11	4315.8	4.0	4335.8	2.1	1.5	36.8	3.92	9.38	0.45	433	0.11	0.9403	0.36	69.13	0.40	0.53348	0.14	0.94
ZR-8 (R)	4316.8	4.2	4331.6	2.0	4338.5	1.5	0.50	99.9	1.03	96.85	0.43	4307	0.11	0.9536	0.13	70.23	0.20	0.53443	0.096	0.88
ZR-11 (R)	4313.8	5.0	4329.6	2.2	4336.9	1.3	0.53	88.5	0.45	195.13	0.45	8639	0.11	0.9526	0.16	70.09	0.22	0.53387	0.085	0.93
ZR-1 (L2)	3715	12	4118.4	4.6	4321.6	2.6	14	11.0	1.35	8.10	0.41	379	0.11	0.7793	0.41	56.74	0.46	0.52832	0.17	0.92
ZR-4 (L2)	4469	19	4373.4	6.5	4329.5	4.1	-3.2	8.66	2.43	3.57	0.45	177	0.11	1.0003	0.58	73.23	0.65	0.5312	0.28	0.90
ZR-5 (L2)	3328	14	3944.3	6.5	4274.0	5.7	22	16.4	4.15	3.96	0.39	197	0.10	0.6759	0.55	47.64	0.66	0.5115	0.39	0.80
ZR-7 (L2)	4313.7	6.7	4306.6	2.7	4303.4	1.6	0.24	23.1	0.91	25.50	0.48	1148	0.12	0.9526	0.21	68.51	0.27	0.52181	0.10	0.92
ZR-8 (L2)	3368.5	8.1	3964.7	3.7	4281.6	2.7	21	19.1	1.40	13.62	0.43	626	0.12	0.6863	0.31	48.63	0.37	0.51415	0.18	0.87
ZR-10 (L2)	3954.9	6.0	4160.1	2.5	4260.8	1.5	7.2	26.7	0.34	77.66	0.53	3457	0.14	0.8469	0.20	59.16	0.25	0.50691	0.094	0.93

[a] Corrected for initial Th/U disequilibrium using radiogenic ^{208}Pb and Th/U[magma] = 3.5. Note that dates uncorrected for Th/U disequilbrium are indistinguishable from these values.

[b] Isotopic dates calculated using $\lambda^{238} = 1.55125 \times 10\text{-}10$ (Jaffey et al. 1971) and $\lambda^{235} = 9.8485 \times 10\text{-}10$ (Jaffey et al. 1971).

[c] % discordance = 100 - (100 * ($^{206}Pb/^{238}U$ date) / ($^{207}Pb/^{206}Pb$ date))

[d] Total mass of radiogenic Pb.

[e] Total mass of common Pb.

[f] Ratio of radiogenic Pb (including ^{208}Pb) to common Pb.

[g] Th contents calculated from radiogenic ^{208}Pb and ^{230}Th-corrected $^{206}Pb/^{238}U$ date of the sample, assuming concordance between U-Pb and Th-Pb systems.

[h] Measured ratio corrected for fractionation and tracer contribution only.

[i] Measured ratios corrected for fractionation, tracer and blank.

Table 2. Sm-Nd Isotope Data for 15405 QMD Clast B

Mineral Fraction	Wt. (mg)	Sm (ppm)	Nd (ppm)	$^{147}Sm/^{144}Nd$	± [a]	$^{143}Nd/^{144}Nd$ [b]	± [c,d]	$^{142}Nd/^{144}Nd$	± [c,d]
Felsic-1	6.96	1.26	4.52	0.16919	0.00017	0.511835	0.000006	1.141816	0.000015
Felsic-2	3.94	7.49	23.7	0.19069	0.00019	0.512451	0.000004	1.141820	0.000010
Mg-Px-1 (L)	---	---	---	0.16021	0.00016	0.511577	0.000001	1.141806	0.000008
Mg-Px-1	11.19	7.25	19.6	0.22338	0.00022	0.513295	0.000003	1.141816	0.000010
Mg-Px-2	6.93	5.43	17.3	0.19023	0.00019	0.512443	0.000004	1.141823	0.000012
Int-Px	4.73	11.7	30.9	0.23042	0.00023	0.513526	0.000003	1.141829	0.000009
Fe-Px	6.5	11.6	30.9	0.22642	0.00023	0.513395	0.000004	1.141831	0.000010
Wr-1	5.79	34.0	124.2	0.16537	0.00017	0.511729	0.000002	1.141806	0.000008
JNdi (N = 6)						0.512103	0.000004	1.141836	0.000008

[a] Reported uncertainties (2σ) refer to the last significant digits and include a minimum 0.1% uncertainty for $^{147}Sm/^{144}Nd$ plus a 50% uncertainty on the blank correction.

[b] $^{143}Nd/^{144}Nd$ values are internally normalized to $^{146}Nd/^{144}Nd = 0.7219$. Samples were run as Nd^+.

[c] Reported uncertainties on $^{143}Nd/^{144}Nd$ reflect twice the standard error (2s.e.) based on internal run statistics on a cycle-by-cycle basis of an individual sample.

[d] Reported uncertainty (2σ) on $^{143}Nd/^{144}Nd$ standard runs denote the last significant digits and represents twice the standard deviation (2s.d.) from replicate analyses (N = 6) of JNdi.

Table 3. Rb-Sr Isotope Data for 15405 QMD Clast B

Mineral Fraction	Wt. (mg)	Rb (ppm)	Sr (ppm)	$^{87}Rb/^{86}Sr$	± [a]	$^{87}Sr/^{86}Sr$ [b]	± [c,d]
Felsic-1	6.96	41.6	175.4	0.68609	0.00069	0.704560	0.000004
Felsic-2	3.94	40.8	189.4	0.62355	0.00624	0.736319	0.000004
Mg-Px-1 (L)	---	---	---	0.08924	0.00089	0.730052	0.000015
Mg-Px-1	11.19	16.4	52.1	0.91248	0.00912	0.724838	0.000004
Mg-Px-2	6.93	50.5	195.6	0.74661	0.00747	0.746084	0.000004
Int-Px	4.73	18.6	40.3	1.3381	0.0134	0.753478	0.000004
Fe-Px	6.5	18.3	38.2	1.3888	0.0139	0..753478	0.000004
Wr-1	5.79	42.4	186.7	0.657	0.00657	0.741271	0.000004
NBS 987 (N = 8)						0.710252	0.000010

[a] Reported uncertainties (2σ) refer to the last significant digits and include a minimum 1% uncertainty for $^{87}Rb/^{86}Sr$, plus a 50% uncertainty on the blank correction.

[b] Sr isotopic ratios to $^{86}Sr/^{88}Sr = 0.1194$. All Sr isotope analyses were measured as Sr^+.

[c] Reported uncertainties on $^{87}Sr/^{86}Sr$ reflect twice the standard error (2s.e.) based on internal run statistics on a cycle-by-cycle basis of an individual sample.

[d] Reported uncertainty (2σ) on $^{87}Sr/^{86}Sr$ standard runs denote the last significant digits and represents twice the standard deviation (2s.d.) from replicate analyses (N = 8) of NBS-987.

Table 4. SIMS Pb-Pb Data for Baddeleyite in MGS samples 78236 and 78255

File	$^{207}Pb/^{206}Pb$ age (Ma)	± 1σ	$^{206}Pb/^{238}U$ age (Ma)	± 1σ	$^{207}Pb/^{235}U$ age (Ma)	± 1σ	radiogenic ^{206}Pb (%)
78238_zr7_badde_2nA@1.ais	4330	7.8	4538	225	4395	70	99.37
78238_zr7_badde_2nA@2.ais	4338	7.8	4283	175	4320	57	98.73
78238_zr7_badde_2nA@3.ais	4327	12.5	4458	177	4368	55	99.68
78238_zr5_badde_2nA@1.ais	4341	20.9	4412	212	4364	67	99.36
78238_zr6_badde_2nA@1.ais	4327	7.5	4182	147	4280	48	99.43
78238_zr2_badde_2nA@1.ais	4332	3.1	4490	156	4382	49	99.96
78238_zr3_badde_2nA@1.ais	4315	7.7	4729	331	4443	98	99.75
78238_zr4_badde_2nA@1.ais	4326	17.6	4109	211	4256	74	99.57
78238_zr4_badde_2nA@2.ais	4342	4.4	4477	207	4384	65	99.64
78238_zr4_badde_2nA@3.ais	4329	4.9	4503	199	4383	62	99.67
78255-9-badd@1.ais	4181	98.5	3761	287	4040	95	99.81
78255-9-badd@2.ais	4343	27.2	4120	255	4271	74	99.84
78255-9-badd@3.ais	4358	29.7	5254	112	4624	28	99.73
78255-9-badd@4.ais	4184	150.3	4881	452	4399	97	99.89
78255-9-badd@5.ais	4338	26.2	4213	84	4298	33	99.91
78255-9-badd@5.ais	4338	26.2	4213	84	4298	33	99.91
78255-9-zrc@1.ais	4337	8.3	4484	74	4383	22	99.96
78255-9-zrc@2.ais	4339	7.8	4340	78	4340	24	99.95

Weighted average $^{207}Pb/^{206}Pb$ age of all 18 spots is 4333.9 ± 3.7 Ma (2se; MSWD = 0.72).
$^{207}Pb/^{206}Pb$ age calculated assuming common Pb is terrestrial ($^{206}Pb/^{204}Pb$ = 18.7, $^{206}Pb/^{206}Pb$ = 0.84 (Stacy and Kramers, 1975).

Table 1. U-Pb isotope dilution data for 15405 QMD Clast B zircon residue (R) and leachate (L) fractions.

Sample	Dates (Ma)							Composition				Isotopic Ratios								
	$^{206}Pb/^{238}U$ <Th>[a,b]	±2σ abs	$^{207}Pb/^{235}U$	±2σ abs	$^{207}Pb/^{206}Pb$	±2σ abs	% disc[c]	Pb* (pg) [d]	Pbc (pg) [e]	Pb*/ Pbc [f]	Th/U (Min)	$^{206}Pb/^{204}Pb$ [h]	$^{208}Pb/^{206}Pb$ [i]	$^{206}Pb/^{238}U$ <Th> [i,a]	±2σ %	$^{207}Pb/^{235}U$ [i]	±2σ %	$^{207}Pb/^{206}Pb$ <Th> [i,a]	±2σ %	Corr. Coef.
ZR-1 (R)	4315.2	4.0	4330.3	1.9	4337.3	1.4	0.51	88.1	1.65	53.44	0.39	2398	0.10	0.9531	0.13	70.14	0.19	0.53400	0.089	0.91
ZR-4 (R)	4098	37	4259	12	4336.0	2.7	5.5	28.4	1.08	26.40	0.42	1188	0.11	0.888	1.2	65.31	1.2	0.53353	0.18	0.99
ZR-5 (R)	4273	11	4315.8	4.0	4335.8	2.1	1.5	36.8	3.92	9.38	0.45	433	0.11	0.9403	0.36	69.13	0.40	0.53348	0.14	0.94
ZR-8 (R)	4316.8	4.2	4331.6	2.0	4338.5	1.5	0.50	99.9	1.03	96.85	0.43	4307	0.11	0.9536	0.13	70.23	0.20	0.53443	0.096	0.88
ZR-11 (R)	4313.8	5.0	4329.6	2.2	4336.9	1.3	0.53	88.5	0.45	195.13	0.45	8639	0.11	0.9526	0.16	70.09	0.22	0.53387	0.085	0.93
ZR-1 (L2)	3715	12	4118.4	4.6	4321.6	2.6	14	11.0	1.35	8.10	0.41	379	0.11	0.7793	0.41	56.74	0.46	0.52832	0.17	0.92
ZR-4 (L2)	4469	19	4373.4	6.5	4329.5	4.1	-3.2	8.66	2.43	3.57	0.45	177	0.11	1.0003	0.58	73.23	0.65	0.5312	0.28	0.90
ZR-5 (L2)	3328	14	3944.3	6.5	4274.0	5.7	22	16.4	4.15	3.96	0.39	197	0.10	0.6759	0.55	47.64	0.66	0.5115	0.39	0.80
ZR-7 (L2)	4313.7	6.7	4306.6	2.7	4303.4	1.6	0.24	23.1	0.91	25.50	0.48	1148	0.12	0.9526	0.21	68.51	0.27	0.52181	0.10	0.92
ZR-8 (L2)	3368.5	8.1	3964.7	3.7	4281.6	2.7	21	19.1	1.40	13.62	0.43	626	0.12	0.6863	0.31	48.63	0.37	0.51415	0.18	0.87
ZR-10 (L2)	3954.9	6.0	4160.1	2.5	4260.8	1.5	7.2	26.7	0.34	77.66	0.53	3457	0.14	0.8469	0.20	59.16	0.25	0.50691	0.094	0.93

[a] Corrected for initial Th/U disequilibrium using radiogenic ^{208}Pb and Th/U[magma] = 3.5. Note that dates uncorrected for Th/U disequilbrium are indistinguishable from these values.
[b] Isotopic dates calculated using λ^{238} = 1.55125×10-10 (Jaffey et al. 1971) and λ^{235} = 9.8485×10-10 (Jaffey et al. 1971).
[c] % discordance = 100 - (100 * ($^{206}Pb/^{238}U$ date) / ($^{207}Pb/^{206}Pb$ date))
[d] Total mass of radiogenic Pb.
[e] Total mass of common Pb.
[f] Ratio of radiogenic Pb (including ^{208}Pb) to common Pb.
[g] Th contents calculated from radiogenic ^{208}Pb and ^{230}Th-corrected $^{206}Pb/^{238}U$ date of the sample, assuming concordance between U-Pb and Th-Pb systems.
[h] Measured ratio corrected for fractionation and tracer contribution only.
[i] Measured ratios corrected for fractionation, tracer and blank.

Table 2. Sm-Nd Isotope Data for 15405 QMD Clast B

Mineral Fraction	Wt. (mg)	Sm (ppm)	Nd (ppm)	$^{147}Sm/^{144}Nd$	± [a]	$^{143}Nd/^{144}Nd$ [b]	± [c,d]	$^{142}Nd/^{144}Nd$	± [c,d]
Felsic-1	6.96	1.26	4.52	0.16919	0.00017	0.511835	0.000006	1.141816	0.000015
Felsic-2	3.94	7.49	23.7	0.19069	0.00019	0.512451	0.000004	1.141820	0.000010
Mg-Px-1 (L)	---	---	---	0.16021	0.00016	0.511577	0.000001	1.141806	0.000008
Mg-Px-1	11.19	7.25	19.6	0.22338	0.00022	0.513295	0.000003	1.141816	0.000010
Mg-Px-2	6.93	5.43	17.3	0.19023	0.00019	0.512443	0.000004	1.141823	0.000012
Int-Px	4.73	11.7	30.9	0.23042	0.00023	0.513526	0.000003	1.141829	0.000009
Fe-Px	6.5	11.6	30.9	0.22642	0.00023	0.513395	0.000004	1.141831	0.000010
Wr-1	5.79	34.0	124.2	0.16537	0.00017	0.511729	0.000002	1.141806	0.000008
JNdi (N = 6)						0.512103	0.000004	1.141836	0.000008

[a] Reported uncertainties (2σ) refer to the last significant digits and include a minimum 0.1% uncertainty for $^{147}Sm/^{144}Nd$ plus a 50% uncertainty on the blank correction.

[b] $^{143}Nd/^{144}Nd$ values are internally normalized to $^{146}Nd/^{144}Nd = 0.7219$. Samples were run as Nd^+.

[c] Reported uncertainties on $^{143}Nd/^{144}Nd$ reflect twice the standard error (2s.e.) based on internal run statistics on a cycle-by-cycle basis of an individual sample.

[d] Reported uncertainty (2σ) on $^{143}Nd/^{144}Nd$ standard runs denote the last significant digits and represents twice the standard deviation (2s.d.) from replicate analyses (N = 6) of JNdi.

Table 3. Rb-Sr Isotope Data for 15405 QMD Clast B

Mineral Fraction	Wt. (mg)	Rb (ppm)	Sr (ppm)	$^{87}Rb/^{86}Sr$	± [a]	$^{87}Sr/^{86}Sr$ [b]	± [c,d]
Felsic-1	6.96	41.6	175.4	0.68609	0.00069	0.704560	0.000004
Felsic-2	3.94	40.8	189.4	0.62355	0.00624	0.736319	0.000004
Mg-Px-1 (L)	---	---	---	0.08924	0.00089	0.730052	0.000015
Mg-Px-1	11.19	16.4	52.1	0.91248	0.00912	0.724838	0.000004
Mg-Px-2	6.93	50.5	195.6	0.74661	0.00747	0.746084	0.000004
Int-Px	4.73	18.6	40.3	1.3381	0.0134	0.753478	0.000004
Fe-Px	6.5	18.3	38.2	1.3888	0.0139	0..753478	0.000004
Wr-1	5.79	42.4	186.7	0.657	0.00657	0.741271	0.000004
NBS 987 (N = 8)						0.710252	0.000010

[a] Reported uncertainties (2σ) refer to the last significant digits and include a minimum 1% uncertainty for $^{87}Rb/^{86}Sr$, plus a 50% uncertainty on the blank correction.

[b] Sr isotopic ratios to $^{86}Sr/^{88}Sr = 0.1194$. All Sr isotope analyses were measured as Sr^+.

[c] Reported uncertainties on $^{87}Sr/^{86}Sr$ reflect twice the standard error (2s.e.) based on internal run statistics on a cycle-by-cycle basis of an individual sample.

[d] Reported uncertainty (2σ) on $^{87}Sr/^{86}Sr$ standard runs denote the last significant digits and represents twice the standard deviation (2s.d.) from replicate analyses (N = 8) of NBS-987.

Table 4. SIMS Pb-Pb Data for Baddeleyite in MGS samples 78236 and 78255

File	$^{207}Pb/^{206}Pb$ age (Ma)	± 1σ	$^{206}Pb/^{238}U$ age (Ma)	± 1σ	$^{207}Pb/^{235}U$ age (Ma)	± 1σ	radiogenic ^{206}Pb (%)
78238_zr7_badde_2nA@1.ais	4330	7.8	4538	225	4395	70	99.37
78238_zr7_badde_2nA@2.ais	4338	7.8	4283	175	4320	57	98.73
78238_zr7_badde_2nA@3.ais	4327	12.5	4458	177	4368	55	99.68
78238_zr5_badde_2nA@1.ais	4341	20.9	4412	212	4364	67	99.36
78238_zr6_badde_2nA@1.ais	4327	7.5	4182	147	4280	48	99.43
78238_zr2_badde_2nA@1.ais	4332	3.1	4490	156	4382	49	99.96
78238_zr3_badde_2nA@1.ais	4315	7.7	4729	331	4443	98	99.75
78238_zr4_badde_2nA@1.ais	4326	17.6	4109	211	4256	74	99.57
78238_zr4_badde_2nA@2.ais	4342	4.4	4477	207	4384	65	99.64
78238_zr4_badde_2nA@3.ais	4329	4.9	4503	199	4383	62	99.67
78255-9-badd@1.ais	4181	98.5	3761	287	4040	95	99.81
78255-9-badd@2.ais	4343	27.2	4120	255	4271	74	99.84
78255-9-badd@3.ais	4358	29.7	5254	112	4624	28	99.73
78255-9-badd@4.ais	4184	150.3	4881	452	4399	97	99.89
78255-9-badd@5.ais	4338	26.2	4213	84	4298	33	99.91
78255-9-badd@5.ais	4338	26.2	4213	84	4298	33	99.91
78255-9-zrc@1.ais	4337	8.3	4484	74	4383	22	99.96
78255-9-zrc@2.ais	4339	7.8	4340	78	4340	24	99.95

Weighted average $^{207}Pb/^{206}Pb$ age of all 18 spots is 4333.9 ± 3.7 Ma (2se; MSWD = 0.72).
$^{207}Pb/^{206}Pb$ age calculated assuming common Pb is terrestrial ($^{206}Pb/^{204}Pb$ = 18.7, $^{206}Pb/^{206}Pb$ = 0.84 (Stacy and Kramers, 1975).

Table 1. U-Pb isotope dilution data for 15405 QMD Clast B zircon residue (R) and leachate (L) fractions.

Sample	Dates (Ma)							Composition				Isotopic Ratios								
	$^{206}Pb/^{238}U$ <Th>[a,b]	±2σ abs	$^{207}Pb/^{235}U$	±2σ abs	$^{207}Pb/^{206}Pb$	±2σ abs	% disc[c]	Pb* (pg) [d]	Pbc (pg) [e]	Pb*/ Pbc [f]	Th/U (Min)	$^{206}Pb/^{204}Pb$ [h]	$^{208}Pb/^{206}Pb$ [i]	$^{206}Pb/^{238}U$ <Th> [i,a]	±2σ %	$^{207}Pb/^{235}U$ [i]	±2σ %	$^{207}Pb/^{206}Pb$ <Th> [i,a]	±2σ %	Corr. Coef.
ZR-1 (R)	4315.2	4.0	4330.3	1.9	4337.3	1.4	0.51	88.1	1.65	53.44	0.39	2398	0.10	0.9531	0.13	70.14	0.19	0.53400	0.089	0.91
ZR-4 (R)	4098	37	4259	12	4336.0	2.7	5.5	28.4	1.08	26.40	0.42	1188	0.11	0.888	1.2	65.31	1.2	0.53353	0.18	0.99
ZR-5 (R)	4273	11	4315.8	4.0	4335.8	2.1	1.5	36.8	3.92	9.38	0.45	433	0.11	0.9403	0.36	69.13	0.40	0.53348	0.14	0.94
ZR-8 (R)	4316.8	4.2	4331.6	2.0	4338.5	1.5	0.50	99.9	1.03	96.85	0.43	4307	0.11	0.9536	0.13	70.23	0.20	0.53443	0.096	0.88
ZR-11 (R)	4313.8	5.0	4329.6	2.2	4336.9	1.3	0.53	88.5	0.45	195.13	0.45	8639	0.11	0.9526	0.16	70.09	0.22	0.53387	0.085	0.93
ZR-1 (L2)	3715	12	4118.4	4.6	4321.6	2.6	14	11.0	1.35	8.10	0.41	379	0.11	0.7793	0.41	56.74	0.46	0.52832	0.17	0.92
ZR-4 (L2)	4469	19	4373.4	6.5	4329.5	4.1	-3.2	8.66	2.43	3.57	0.45	177	0.11	1.0003	0.58	73.23	0.65	0.5312	0.28	0.90
ZR-5 (L2)	3328	14	3944.3	6.5	4274.0	5.7	22	16.4	4.15	3.96	0.39	197	0.10	0.6759	0.55	47.64	0.66	0.5115	0.39	0.80
ZR-7 (L2)	4313.7	6.7	4306.6	2.7	4303.4	1.6	0.24	23.1	0.91	25.50	0.48	1148	0.12	0.9526	0.21	68.51	0.27	0.52181	0.10	0.92
ZR-8 (L2)	3368.5	8.1	3964.7	3.7	4281.6	2.7	21	19.1	1.40	13.62	0.43	626	0.12	0.6863	0.31	48.63	0.37	0.51415	0.18	0.87
ZR-10 (L2)	3954.9	6.0	4160.1	2.5	4260.8	1.5	7.2	26.7	0.34	77.66	0.53	3457	0.14	0.8469	0.20	59.16	0.25	0.50691	0.094	0.93

[a] Corrected for initial Th/U disequilibrium using radiogenic ^{208}Pb and Th/U[magma] = 3.5. Note that dates uncorrected for Th/U disequilbrium are indistinguishable from these values.

[b] Isotopic dates calculated using λ^{238} = 1.55125×10-10 (Jaffey et al. 1971) and λ^{235} = 9.8485×10-10 (Jaffey et al. 1971).

[c] % discordance = 100 - (100 * ($^{206}Pb/^{238}U$ date) / ($^{207}Pb/^{206}Pb$ date))

[d] Total mass of radiogenic Pb.

[e] Total mass of common Pb.

[f] Ratio of radiogenic Pb (including ^{208}Pb) to common Pb.

[g] Th contents calculated from radiogenic ^{208}Pb and ^{230}Th-corrected $^{206}Pb/^{238}U$ date of the sample, assuming concordance between U-Pb and Th-Pb systems.

[h] Measured ratio corrected for fractionation and tracer contribution only.

[i] Measured ratios corrected for fractionation, tracer and blank.

Table 2. Sm-Nd Isotope Data for 15405 QMD Clast B

Mineral Fraction	Wt. (mg)	Sm(ppm)	Nd (ppm)	$^{147}Sm/^{144}Nd$	± [a]	$^{143}Nd/^{144}Nd$ [b]	± [c,d]	$^{142}Nd/^{144}Nd$	± [c,d]
Felsic-1	6.96	1.264	4.515	0.16919	0.00017	0.511835	0.000006	1.141816	0.000015
Felsic-2	3.94	7.486	23.733	0.19069	0.00019	0.512451	0.000004	1.141820	0.000010
Mg-Px-1 (L)	---	---	---	0.16021	0.00016	0.511577	0.000001	1.141806	0.000008
Mg-Px-1	11.19	7.25	19.621	0.22338	0.00022	0.513295	0.000003	1.141816	0.000010
Mg-Px-2	6.93	5.434	17.271	0.19023	0.00019	0.512443	0.000004	1.141823	0.000012
Int-Px	4.73	11.761	30.86	0.23042	0.00023	0.513526	0.000003	1.141829	0.000009
Fe-Px	6.5	11.567	30.886	0.22642	0.00023	0.513395	0.000004	1.141831	0.000010
Wr-1	5.79	33.979	124.222	0.16537	0.00017	0.511729	0.000002	1.141806	0.000008
JNdi (N = 6)						0.512103	0.000004	1.141836	0.000008

[a] Reported uncertainties (2σ) refer to the last significant digits and include a minimum 0.1% uncertainty for $^{147}Sm/^{144}Nd$ plus a 50% uncertainty on the blank correction.

[b] $^{143}Nd/^{144}Nd$ values are internally normalized to $^{146}Nd/^{144}Nd = 0.7219$. Samples were run as Nd^{+}.

[c] Reported uncertainties on $^{143}Nd/^{144}Nd$ reflect twice the standard error (2s.e.) based on internal run statistics on a cycle-by-cycle basis of an individual sample.

[d] Reported uncertainty (2σ) on $^{143}Nd/^{144}Nd$ standard runs denote the last significant digits and represents twice the standard deviation (2s.d.) from replicate analyses (N = 6) of JNdi.

Table 3. Rb-Sr Isotope Data for 15405 QMD Clast B

Mineral Fraction	Wt. (mg)	Rb (ppm)	Sr (ppm)	$^{87}Rb/^{86}Sr$	± [a]	$^{87}Sr/^{86}Sr$ [b]	± [c,d]
Felsic-1	6.96	41.6	175.4	0.68609	0.00069	0.70456	0.000004
Felsic-2	3.94	40.8	189.4	0.62355	0.00624	0.736319	0.000004
Mg-Px-1 (L)	---	---	---	0.08924	0.00089	0.730052	0.000015
Mg-Px-1	11.19	16.4	52.1	0.91248	0.00912	0.724838	0.000004
Mg-Px-2	6.93	50.5	195.6	0.74661	0.00747	0.746084	0.000004
Int-Px	4.73	18.6	40.3	1.3381	0.0134	0.753478	0.000004
Fe-Px	6.5	18.3	38.2	1.3888	0.0139	0..753478	0.000004
Wr-1	5.79	42.4	186.7	0.657	0.00657	0.741271	0.000004
NBS 987 (N = 8)						0.710252	0.000010

[a] Reported uncertainties (2σ) refer to the last significant digits and include a minimum 1% uncertainty for $^{87}Rb/^{86}Sr$, plus a 50% uncertainty on the blank correction.

[b] Sr isotopic ratios to $^{86}Sr/^{88}Sr = 0.1194$. All Sr isotope analyses were measured as Sr^{+}.

[c] Reported uncertainties on $^{87}Sr/^{86}Sr$ reflect twice the standard error (2s.e.) based on internal run statistics on a cycle-by-cycle basis of an individual sample.

[d] Reported uncertainty (2σ) on $^{87}Sr/^{86}Sr$ standard runs denote the last significant digits and represents twice the standard deviation (2s.d.) from replicate analyses (N = 8) of NBS-987.

Table 4. SIMS Pb-Pb Data for Baddeleyite in MGS samples 78236 and 78255

File	$^{207}Pb/^{206}Pb$ age (Ma)	± 1σ	$^{206}Pb/^{238}U$ age (Ma)	± 1σ	$^{207}Pb/^{235}U$ age (Ma)	± 1σ	radiogenic ^{206}Pb (%)
78238_zr7_badde_2nA@1.ais	4330	7.8	4538	225	4395	70	99.37
78238_zr7_badde_2nA@2.ais	4338	7.8	4283	175	4320	57	98.73
78238_zr7_badde_2nA@3.ais	4327	12.5	4458	177	4368	55	99.68
78238_zr5_badde_2nA@1.ais	4341	20.9	4412	212	4364	67	99.36
78238_zr6_badde_2nA@1.ais	4327	7.5	4182	147	4280	48	99.43
78238_zr2_badde_2nA@1.ais	4332	3.1	4490	156	4382	49	99.96
78238_zr3_badde_2nA@1.ais	4315	7.7	4729	331	4443	98	99.75
78238_zr4_badde_2nA@1.ais	4326	17.6	4109	211	4256	74	99.57
78238_zr4_badde_2nA@2.ais	4342	4.4	4477	207	4384	65	99.64
78238_zr4_badde_2nA@3.ais	4329	4.9	4503	199	4383	62	99.67
78255-9-badd@1.ais	4181	98.5	3761	287	4040	95	99.81
78255-9-badd@2.ais	4343	27.2	4120	255	4271	74	99.84
78255-9-badd@3.ais	4358	29.7	5254	112	4624	28	99.73
78255-9-badd@4.ais	4184	150.3	4881	452	4399	97	99.89
78255-9-badd@5.ais	4338	26.2	4213	84	4298	33	99.91
78255-9-badd@5.ais	4338	26.2	4213	84	4298	33	99.91
78255-9-zrc@1.ais	4337	8.3	4484	74	4383	22	99.96
78255-9-zrc@2.ais	4339	7.8	4340	78	4340	24	99.95

Weighted average $^{207}Pb/^{206}Pb$ age of all 18 spots is 4333.9 ± 3.7 Ma (2se; MSWD = 0.72). $^{207}Pb/^{206}Pb$ age calculated assuming common Pb is terrestrial ($^{206}Pb/^{204}Pb$ = 18.7, $^{206}Pb/^{206}Pb$ = 0.84 (Stacy and Kramers, 1975).

Table S1. Representative Composition of Minerals from 15405 QMD Clast B

Mineral	SiO_2	TiO_2	Al_2O_3	FeO	MnO	MgO	CaO	Na_2O	K_2O	Cr_2O_3	Total	En	Fs	Wo	Mg#	An	Ab
Px-1a	48.63	0.41	0.36	34.93	0.59	9.96	4.95	0.02		0.22	100.07	30.7	58.3	11.0	33.7		
Px-1b	49.49	0.92	1.48	20.13	0.34	8.56	18.14	0.11		0.34	99.51	25.8	34.9	39.3	43.1		
Px-1c	48.42	0.73	0.71	27.49	0.45	9.30	12.10	0.05		0.44	99.69	28.6	44.6	26.8	37.6		
Px-2a	49.72	0.90	1.36	20.35	0.30	8.75	18.29	0.12		0.34	100.13	26.2	34.3	39.4	43.4		
Px-2b	48.69	0.54	0.49	32.36	0.49	9.60	7.83	0.03		0.29	100.32	29.6	56.6	13.8	33.8		
Px-3a	49.05	1.05	2.00	19.30	0.30	8.51	19.00	0.13		0.40	99.74	25.9	32.6	41.5	44.0		
Px-3b	48.92	0.30	0.47	38.26	0.58	9.97	1.38	0.01		0.13	100.02	30.6	66.3	3.0	31.7		
Kspar 1a	66.73		18.24	0.23			0.31	0.66	13.86		100.03					1.7	6.6
Kspar 1b	66.25		18.47	0.27			0.29	0.58	14.25		100.11					1.6	5.7
Plag 1a	46.98	0.05	33.45	0.78			16.78	1.81	0.10		99.95					77.0	20.7
Plag 1b	47.18	0.01	33.99	0.19			16.88	1.72	0.06		100.03					84.1	15.5
Plag 2	46.29	0.01	34.19	0.13			17.60	1.41	0.07		99.70					87.0	12.6
Oliv 1	31.51	0.07	0.32	57.83	0.62	8.57	0.65			0.05	99.62						
Oliv 2	31.06	0.04	0.08	62.05	0.67	5.39	0.56			0.05	99.90						
Ilm 1	0.07	52.86	0.08	44.09	0.51	1.34				0.37	99.32						
Ilm 2	0.14	52.96	0.11	43.65	0.54	1.29				0.35	99.04						

Table S2. Major and Trace Element Abundances QMD Clast B Mineral Fractions

Sample	Felsic-1	Felsic-2	Mg-Px-1	Mg-Px-2	Int-Px	Fe-Px	Wr-1
SiO_2 (wt%) [a]	76.11	69.61	74.6	68.98	59.38	58.24	63.67
TiO_2	0.1	0.42	0.38	0.8	0.63	0.67	0.67
Al_2O_3	14.6	15.46	4.49	15.63	3.48	3.4	15.28
FeO*	0.19	3.43	10.06	3.43	20.07	21.36	6.5
MnO	0	0.05	0.16	0.05	0.31	0.33	0.09
MgO	0.03	0.78	3.34	0.77	6.45	6.69	1.72
CaO	5.88	7.51	6.1	7.14	8.85	8.51	8.56
Na_2O	1.14	1.18	0.38	1.15	0.29	0.25	1.21
K_2O	1.93	1.44	0.42	1.96	0.42	0.43	1.71
P_2O_5	0.02	0.12	0.07	0.08	0.11	0.11	0.59
La (ppm)	4.67	15.5	10.1	12.1	14.7	15.7	85.1
Ce	9.28	38.85	27.43	29.2	41.3	43.4	223
Pr	1.14	5.36	4.13	3.96	6.34	6.53	28.6
Nd	4.66	23.9	20.1	17.6	31.2	31.7	126.4
Sm	1.33	7.51	7.5	5.54	11.9	11.8	34.7
Eu	2.48	2.59	0.77	2.7	0.64	0.62	2.74
Gd	1.44	9.04	9.73	6.7	15.8	15.7	39.1
Tb	0.3	1.93	2.21	1.44	3.64	3.65	7.11
Dy	1.96	13.67	16.2	10.4	27.3	27.3	44.5
Ho	0.43	3.02	3.64	2.32	6.18	6.27	9.13
Er	1.32	9.57	11.8	7.6	20.3	20.9	26.1
Tm	0.21	1.52	1.93	1.24	3.36	3.52	3.67
Yb	1.59	10.5	13.6	8.85	24.3	25.3	23
Lu	0.2	1.51	2.09	1.31	3.78	4.02	3.17
Rb	38.9	36.7	15.4	46.2	16.9	16.5	40.1
Sr	182	193	54.8	197	41.5	40.5	192.5
Y	10.7	77.4	95.8	60.1	163	166	249
Zr	116	358	179	510	222	260	407
Nb	7.8	41.7	13.4	68.1	17.9	24.3	51.9
Ba	1630	1252	367	1632	326	310	1431
Hf	3.29	10	5.53	14.4	7.04	8.05	11.1
Ta	0.56	2.3	0.62	3.23	0.9	0.98	2.35
Th	5.07	15.7	4.81	12.9	5.46	6.28	16.6
Ni	0.46	0.43	0.11	0.1	0.1	0.18	16.7
Cr	11.2	213	839	291	1477	1392	465
Co	0.09	2	6.2	2.1	13	13.7	5.8
Sc	0.32	8.4	29.8	8.1	55.1	55.5	15.2

[a] SiO_2 calculated by difference

Table S3. U-Pb isotope dilution data for Temora-2 zircon standards.

Sample	Dates (Ma)							Composition				Isotopic Ratios								
	$^{206}Pb/^{238}U$ <Th>[a,b]	±2σ abs	$^{207}Pb/^{235}U$	±2σ abs	$^{207}Pb/^{206}Pb$	±2σ abs	% disc[c]	Pb* (pg) [d]	Pbc (pg) [e]	Pb*/ Pbc [f]	Th/U (Min)	$^{206}Pb/^{204}Pb$ [h]	$^{208}Pb/^{206}Pb$ [i]	$^{206}Pb/^{238}U$ <Th> [i,a]	±2σ %	$^{207}Pb/^{235}U$ [i]	±2σ %	$^{207}Pb/^{206}Pb$ <Th> [i,a]	±2σ %	Corr. Coef.
TM-1	416.87	0.81	417.15	0.87	418.7	2.4	0.57	188	0.65	288	0.48	17407	0.15	0.06680	0.20	0.5081	0.25	0.055184	0.10	0.92
TM-2	417.35	0.33	416.97	0.63	414.9	2.5	-0.45	226	1.32	171	0.45	10405	0.14	0.066883	0.083	0.50781	0.18	0.055090	0.11	0.93
TM-3	417.55	0.35	417.42	0.65	416.7	2.6	-0.058	140	0.84	166	0.40	10282	0.13	0.066916	0.086	0.50847	0.19	0.055135	0.11	0.92
TM-4	417.60	0.37	417.50	0.63	417.0	2.5	-0.010	243	1.07	228	0.40	14074	0.12	0.066925	0.092	0.50860	0.18	0.055142	0.11	0.88
TM-5	417.37	0.38	416.7	1.0	413.1	5.1	-0.90	118	1.88	63	0.47	3823	0.15	0.066887	0.094	0.5074	0.29	0.05505	0.22	0.79
TM-6	417.37	0.43	417.27	0.81	416.7	3.8	-0.017	120	1.01	119	0.48	7194	0.15	0.066887	0.11	0.5083	0.24	0.055136	0.16	0.77
TM-7	417.71	0.36	417.34	0.81	415.3	3.6	-0.44	60.6	0.78	77	0.36	4844	0.11	0.066942	0.090	0.5083	0.24	0.055100	0.16	0.89
TM-8	416.82	0.35	416.92	0.75	417.5	3.5	0.30	63.9	0.63	102	0.30	6486	0.10	0.066795	0.086	0.5077	0.22	0.055154	0.15	0.83
TM-9	417.58	0.36	417.99	0.85	420.3	4.3	0.79	67.9	1.17	58	0.28	3726	0.09	0.066921	0.088	0.5093	0.25	0.05522	0.19	0.72
TM-10	416.81	0.36	417.21	0.85	419.4	4.2	0.76	203	3.31	61	0.47	3712	0.15	0.066794	0.089	0.5082	0.25	0.05520	0.18	0.79
TM-11	417.02	0.61	417.8	1.3	422.2	7.1	1.4	182	5.77	32	0.37	1974	0.12	0.06683	0.15	0.5090	0.37	0.05527	0.32	0.54
TM-12	417.05	0.46	416.93	0.88	416.2	4.4	-0.056	162	2.44	66	0.48	4035	0.15	0.066834	0.11	0.5077	0.26	0.05512	0.20	0.68
TM-13	417.28	0.45	417.01	0.84	415.5	3.7	-0.27	126	1.42	89	0.33	5613	0.10	0.066871	0.11	0.5079	0.25	0.055106	0.16	0.82
TM-14	416.62	0.78	416.7	1.4	417.4	7.2	0.33	89.0	1.39	64	0.32	4067	0.10	0.06676	0.19	0.5075	0.40	0.05515	0.32	0.61
TM-15	417.46	0.39	417.08	0.62	414.9	2.2	-0.47	400	0.78	512	0.37	31801	0.12	0.066902	0.097	0.50796	0.18	0.055091	0.092	0.93
TM-16	417.84	0.76	417.54	0.87	415.9	2.7	-0.32	120	0.92	131	0.52	7807	0.16	0.06696	0.19	0.5087	0.25	0.055116	0.12	0.89
TM-17	417.82	0.99	417.5	1.1	415.9	3.8	-0.30	158	1.12	142	0.28	9043	0.09	0.06696	0.24	0.5086	0.31	0.055116	0.16	0.85

a Corrected for initial Th/U disequilibrium using radiogenic ^{208}Pb and Th/U[magma] = 3.5.

b Isotopic dates calculated using λ^{238} = 1.55125×10-10 (Jaffey et al. 1971) and λ235 = 9.8485×10-10 (Jaffey et al. 1971).

c % discordance = 100 - (100 * ($^{206}Pb/^{238}U$ date) / ($^{207}Pb/^{206}Pb$ date))

d Total mass of radiogenic Pb.

e Total mass of common Pb.

f Ratio of radiogenic Pb (including ^{208}Pb) to common Pb.

g Th contents calculated from radiogenic ^{208}Pb and ^{230}Th-corrected $^{206}Pb/^{238}U$ date of the sample, assuming concordance between U-Pb and Th-Pb systems.

h Measured ratio corrected for fractionation and tracer contribution only.

i Measured ratios corrected for fractionation, tracer and blank.

Table S4. Effect of varying Pb blank contributions and compositions on $^{207}Pb/^{206}Pb$ ages of 15405 QMD Clast B zircons

Zircon R fraction	$^{207}Pb/^{206}$ Pb age (Ma)	±	$^{207}Pb/^{206}Pb$ age (Ma)	±	$^{207}Pb/^{206}Pb$ age (Ma)	±	Pb_c	Pb^*/Pb_c
	(Modern Pb only)		(Modern + SK75 Pb)		(Modern + high-μ Pb)			
ZR-1	4337.2	1.4	4337.0	1.4	4332.7	4.1	1.63	54
ZR-4	4335.7	2.8	4335.6	2.8	4333	12	1.06	27
ZR-5	4335.1	3.0	4333.7	1.8	4289.5	9.7	3.87	9.5
ZR-8	4338.4	1.5	4338.4	1.5	4337.9	3.7	1.02	98
ZR-11	4336.9	1.3	4336.9	1.3	4336.9	1.3	0.45	197

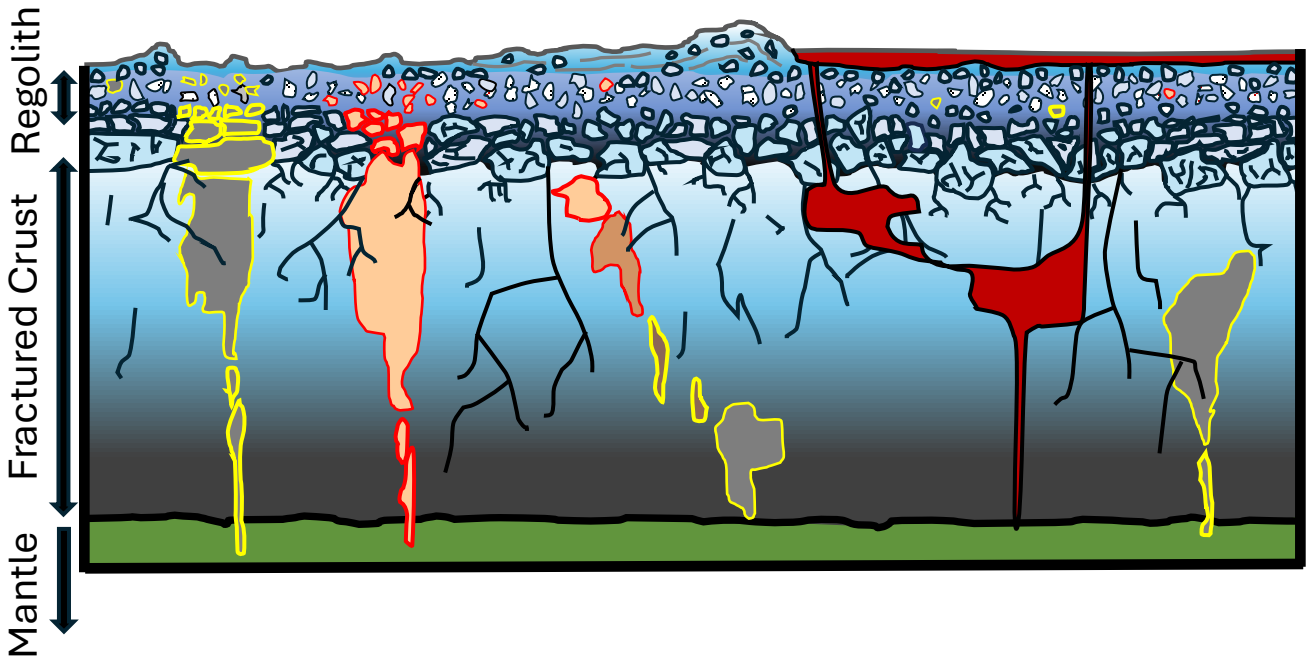

Stratigraphy Based on Petrology

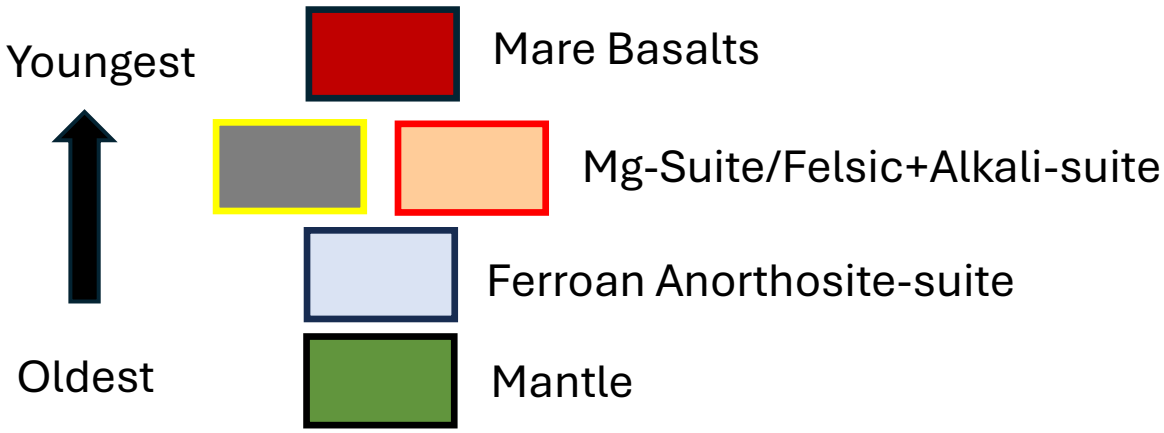

Figure 1

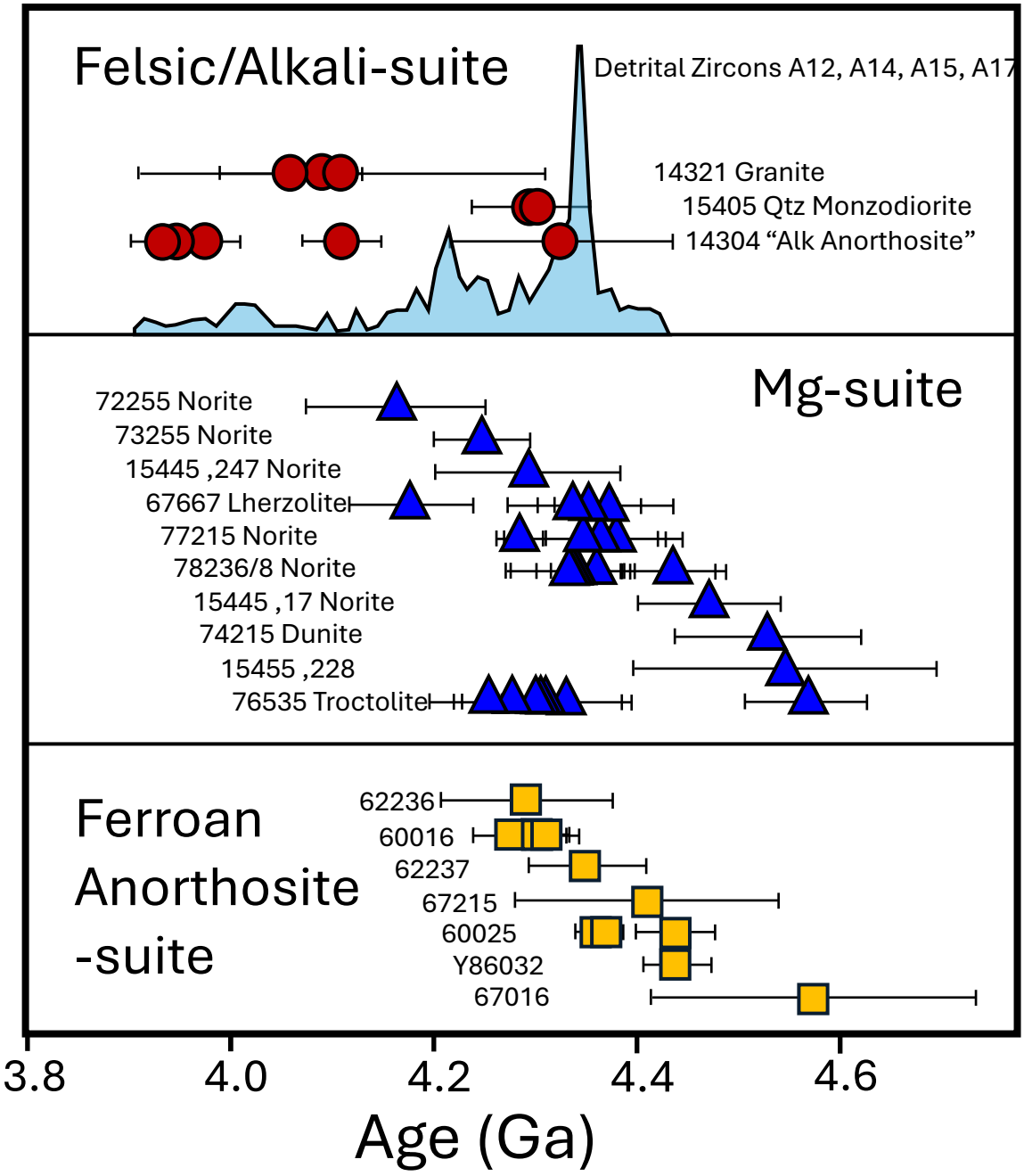

Figure 2

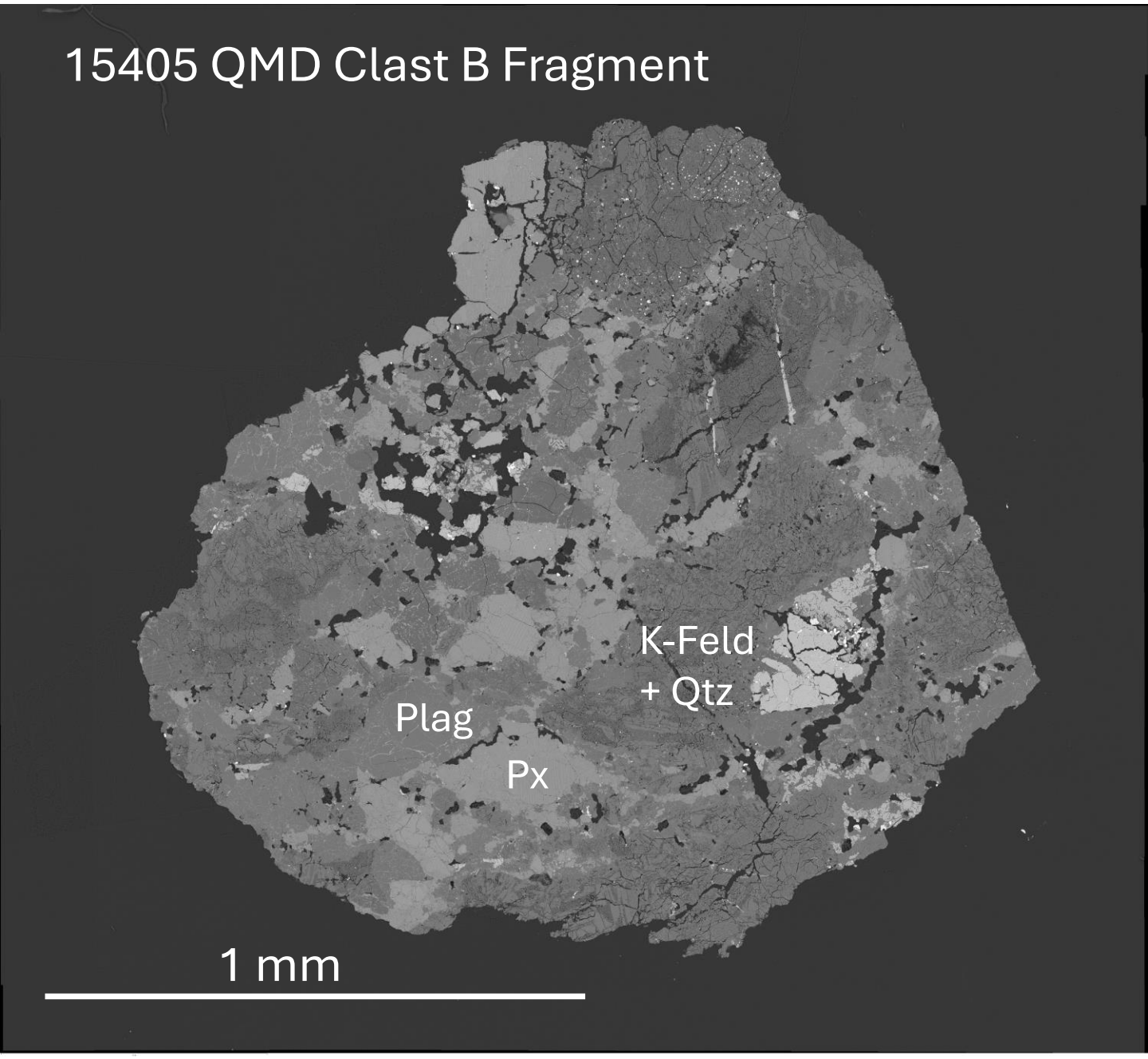

Figure 3

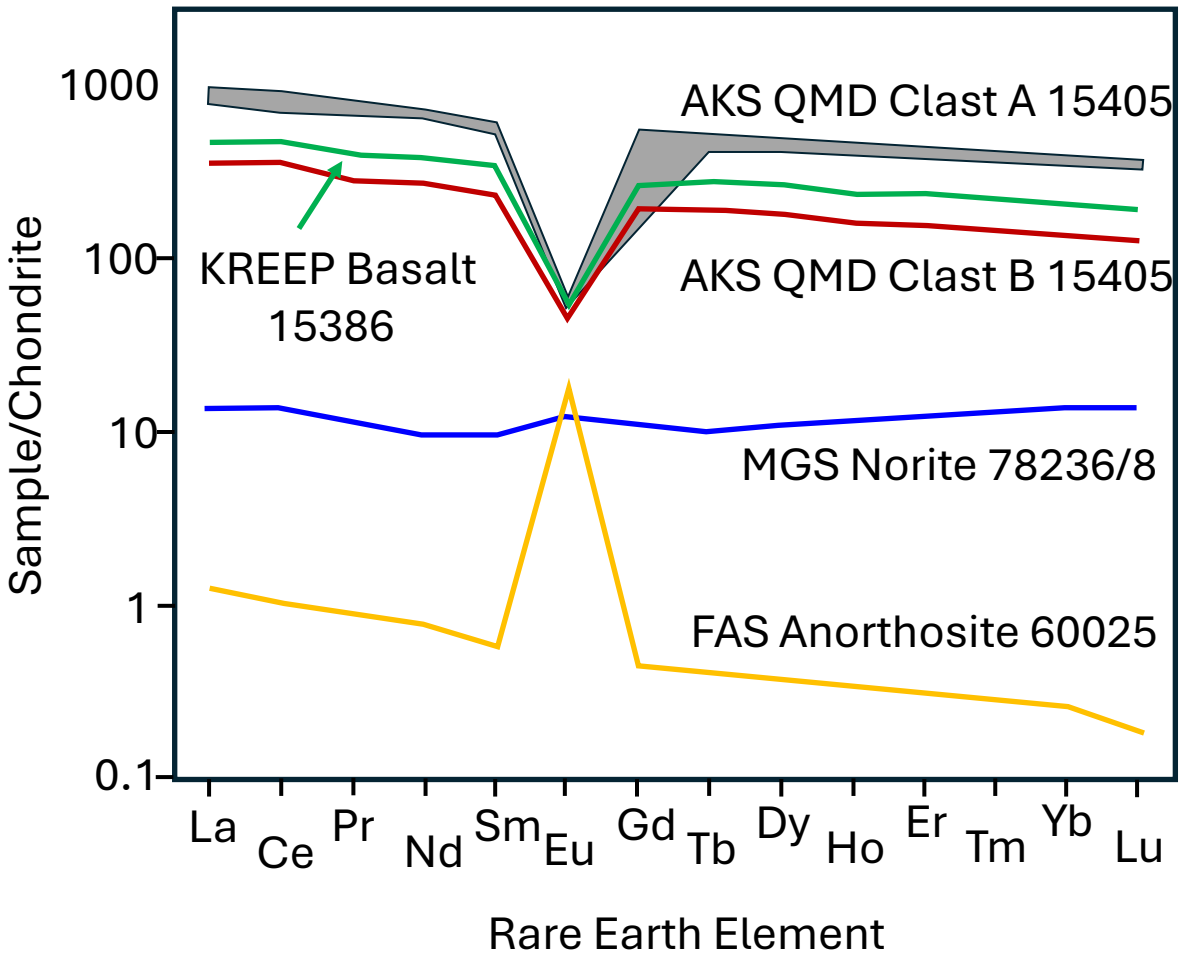

Figure 4

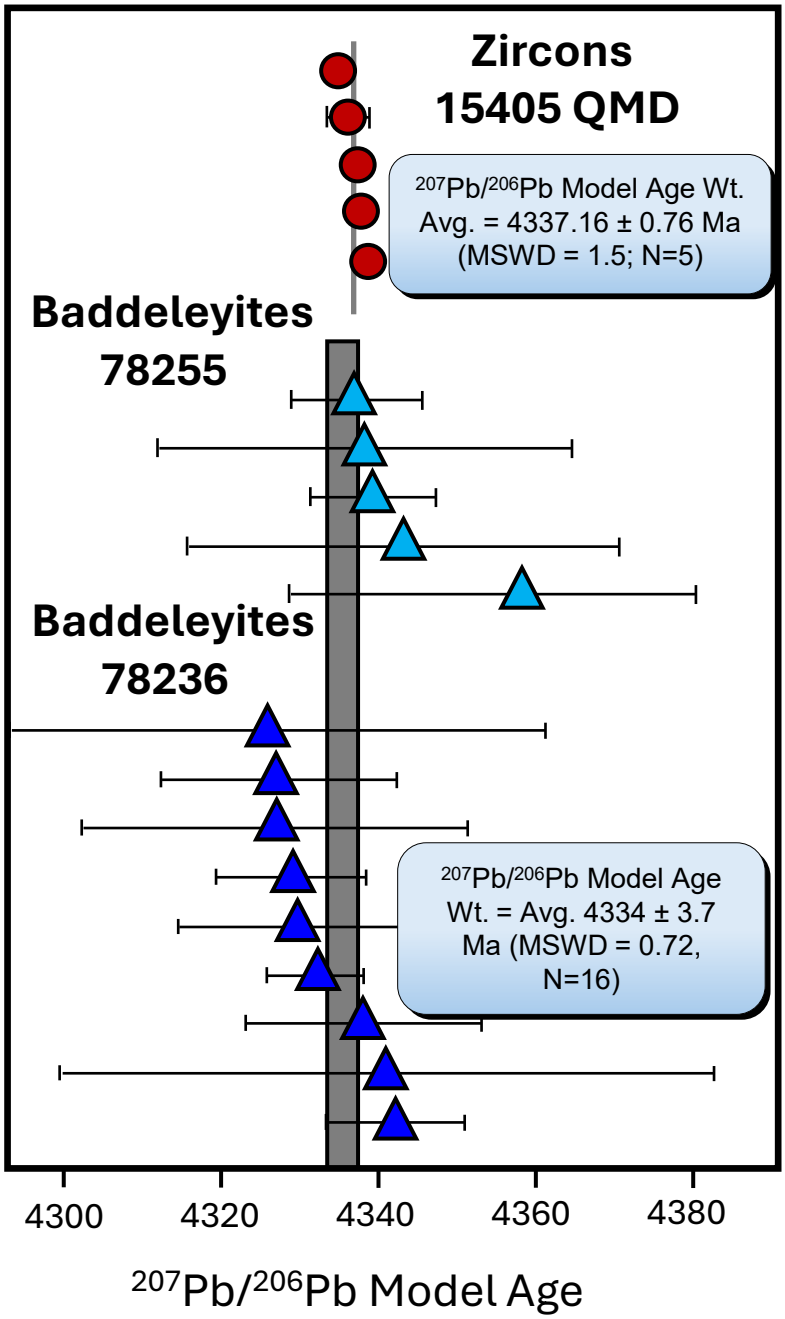

Figure 5

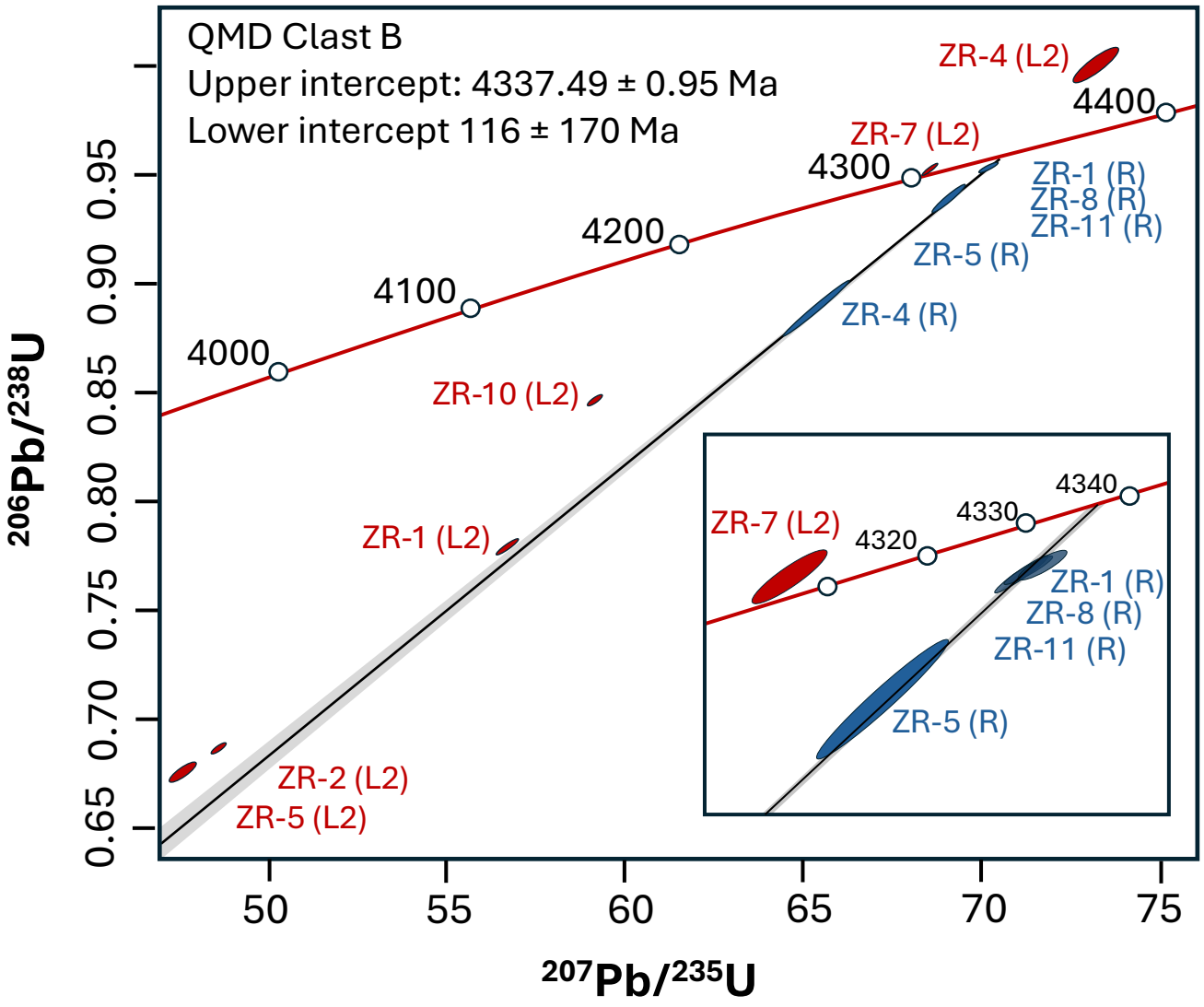

Figure 6

Figure 7

Click here to access/download;Figure;Figure 7.pdf

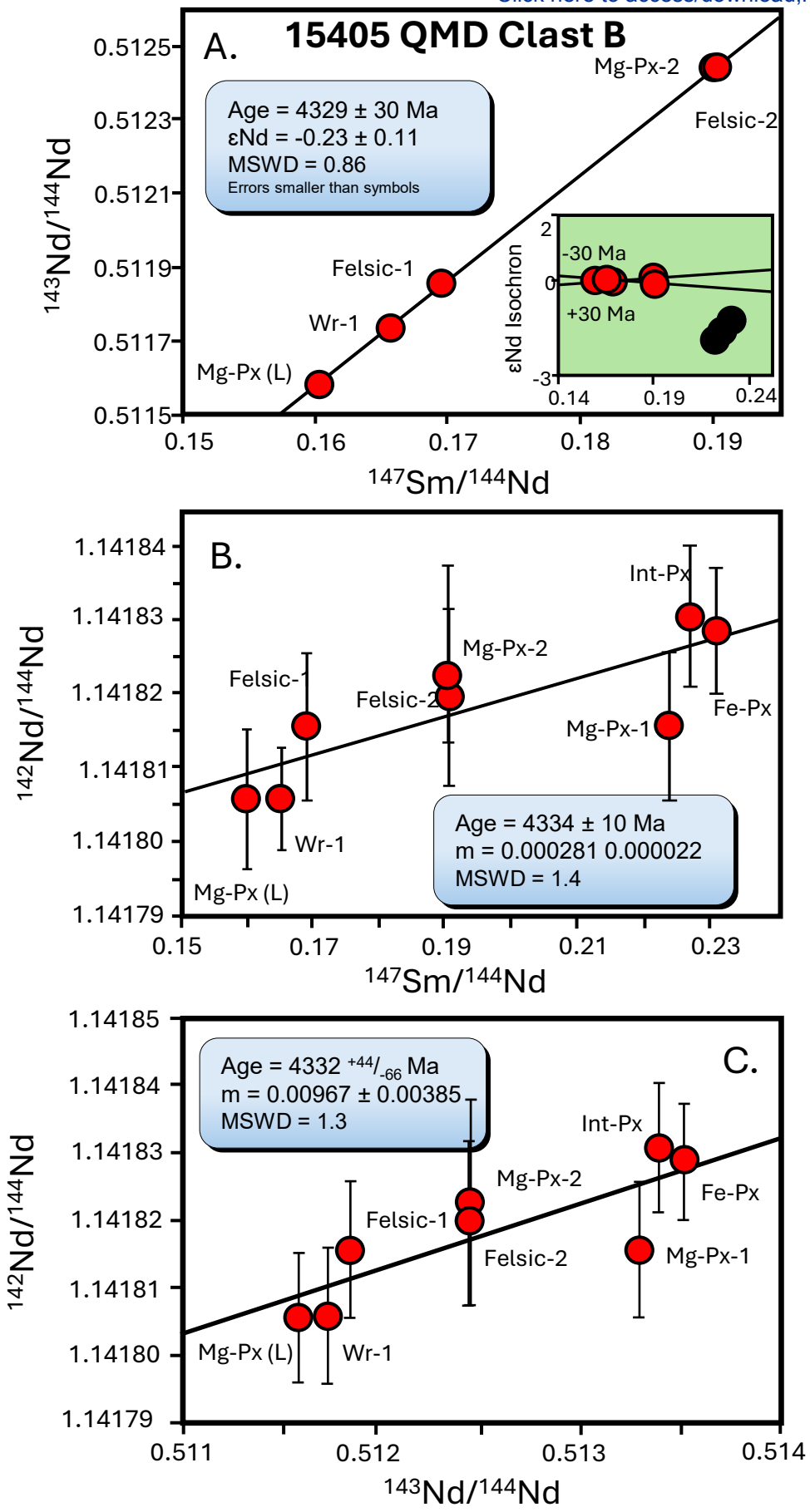

Figure 7

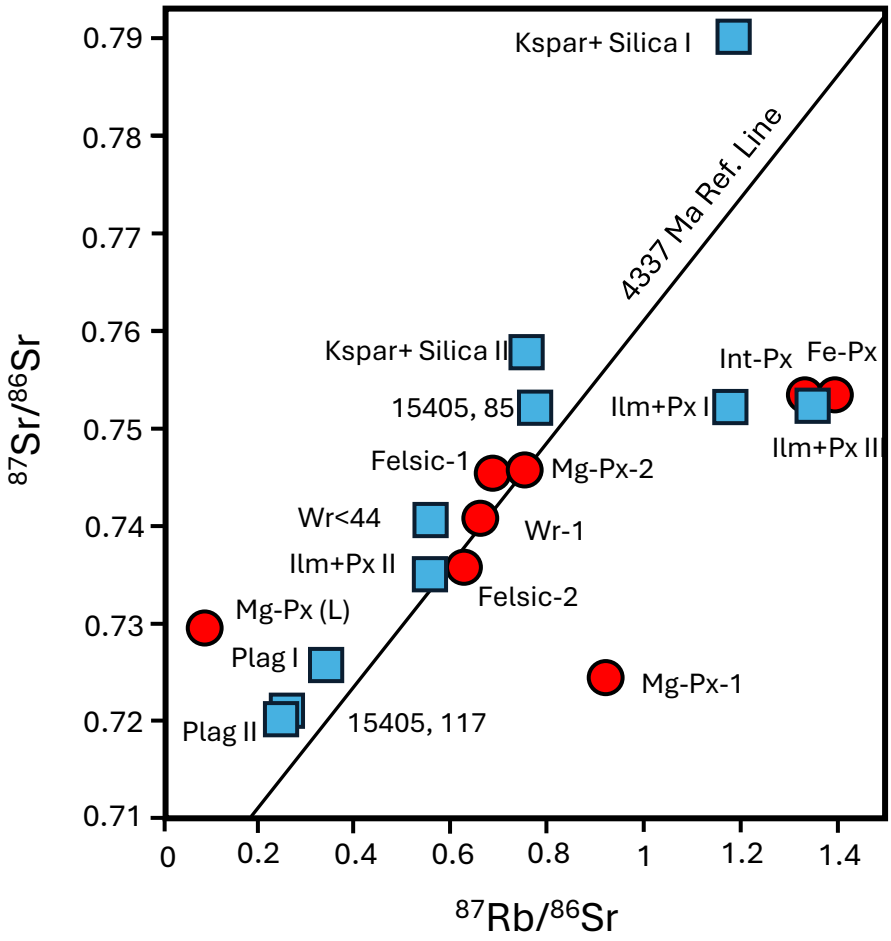

Figure 8

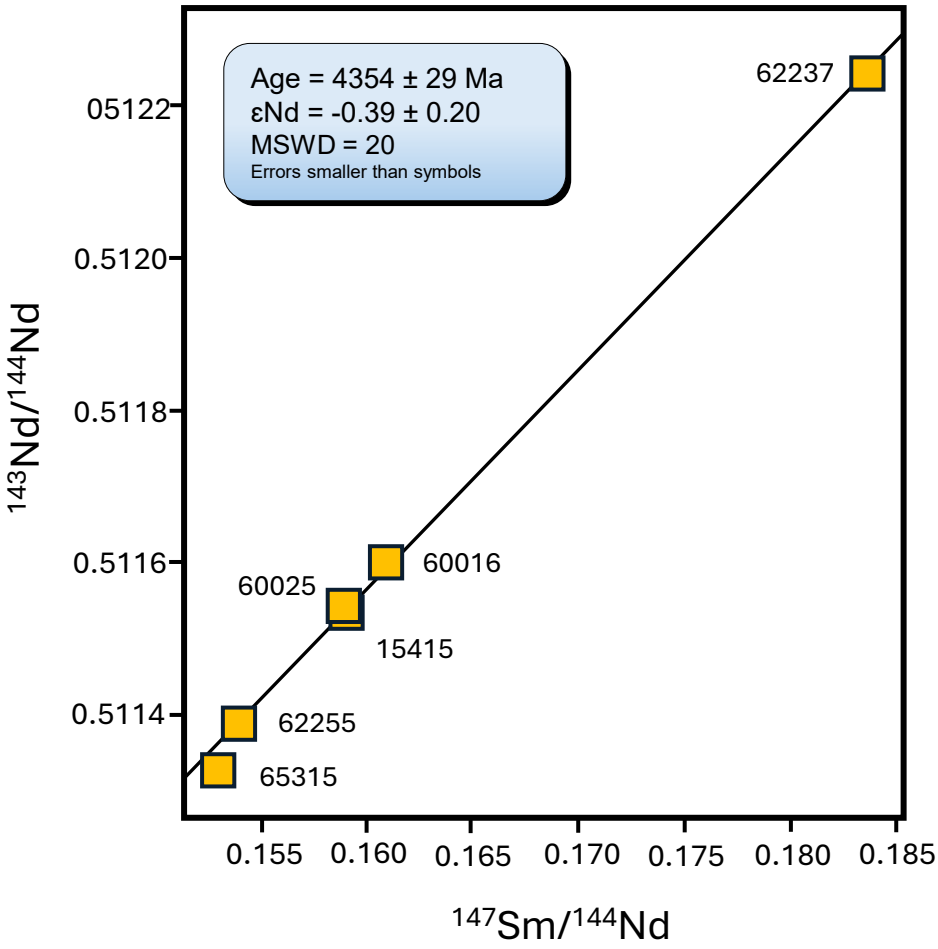

Figure 9

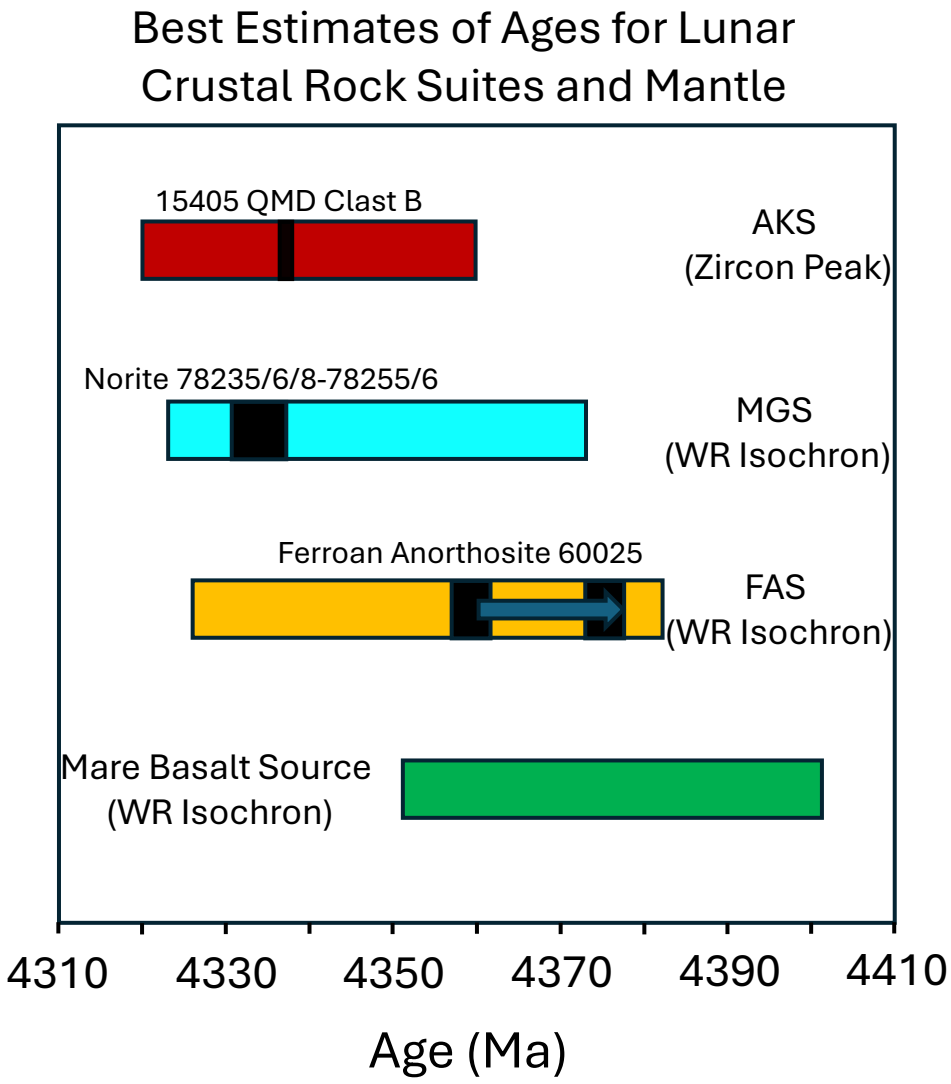

Figure 10

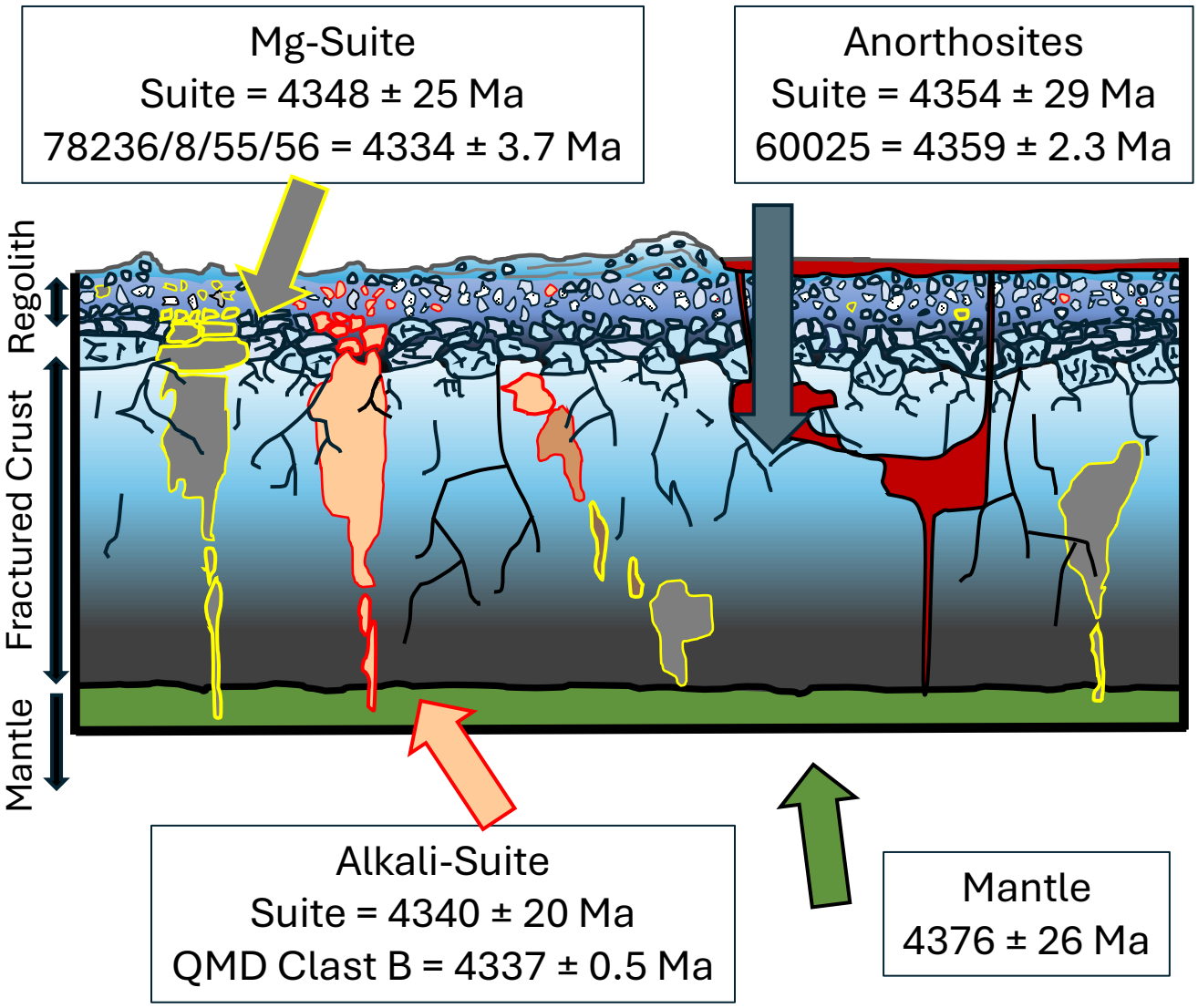

Figure 11